CHAPTER-IV

STRUCTURES

4.1 Introduction

In the area, due to lake of continuity of the exposures, thick forest and soil cover structural features are not easily discernable. However, sufficient care has been taken during field investigation judiciously to work out the structural fabrics and structural configuration in the area.

The whole area of study is composed of multi-deformed metasedimentary rocks where we find significant intrusion of granites and epidiorites (Khasi greenstone). These sequences of the Shillong Group of rocks metamorphosed to epidote-amphibolite facies condition. Hence, various conspicuous structural features have been noticed in the rocks of the area.

Both non-diastrophic (primary) and diastrophic (secondary) structures are present in the area. The strike of the Shillong Group of rocks is NE-SW. In the present study area dip of the bedding planes and foliations towards NW in the eastern part and towards SE in the western part, thus, indicating a synclinal structure (Map.1).

From the systematic study of the fields, planer and linear structures in the rocks of the study area reveals that the metasedimentary rocks of the Shillong Group have been affected by four phases of deformation (D) leading to the

development of folding (F_1,F_2&F_3) with their contemporaneous planer (S_1,S_2&S_3) and linear (L_1,L_2&L_3) structures.

4.2 Non-diastrophic structures (Primary)

The non-diastrophic structures observed in the rocks of the Shillong Group are of planar and linear structures.

4.2.1 Planar structures

The primary planar structures include bedding planes (S_0), current beddings and graded beddings.

4.2.1.1 Bedding planes (Lithological layering, S_0)

The current bedded quartzites and the presence of conglomerate bed in the formation, which are characteristics of sedimentary rocks, are considered here as 'S_0'. They constitute the primary planar structure. Bedding plane is easily recognized in the field with the following criteria.

- Colour banding in the metasediments.
- Intraformational conglomerate bands in quartzites.
- Thin discontinuous bands of phyllite in quartzites.
- Disposition of pebbles in conglomerate. (Fig.-4.1)
- Current bedding structure in quartzites. (Fig.-4.2,Photo-4.1a)
- Lithological contact between quartzites– phyllite.and conglomerate–quartzites (Photo- 4.1b, Photo- 4.1c)

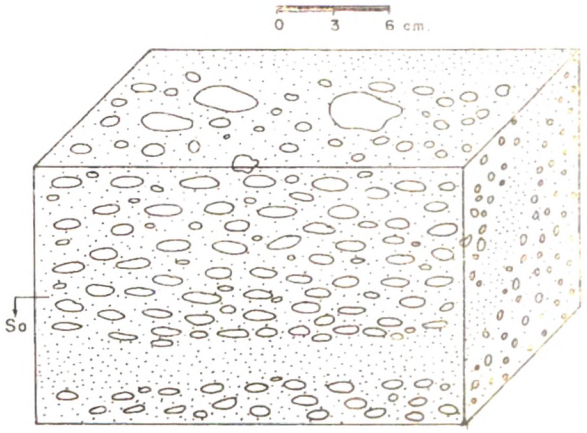

Fig.4.1—Exposure of Conglomerate near Mawryngkneng.

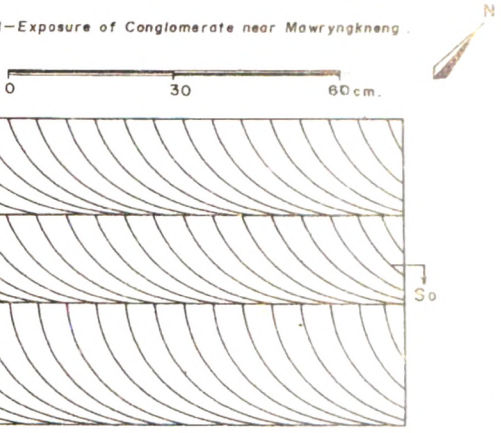

Fig.4.2—Current Bedding in Quartzite exposed on the bed of the river at Ksepangdong.

Photo-4.1a: current bedding in quartzite exposed on the bed of the river at Ksehpongdeng

Photo-4.1b: Lithological contact between quartzite and phyllite on the road cutting at Lulang.

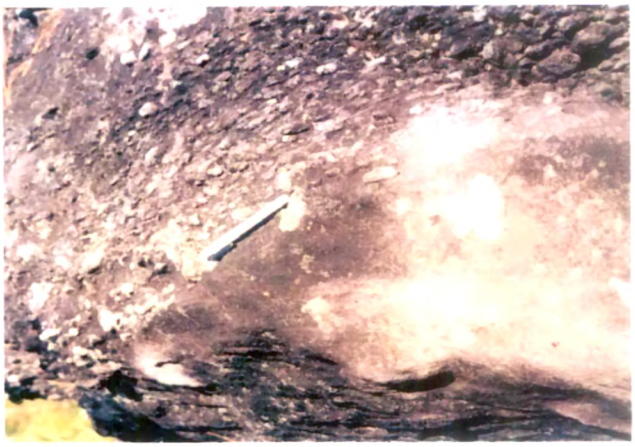

Photo-4.1c: Lithological contact between quartzite and conglomerate exposed at Lulang.

The intraformational conglomerates are well exposed in and around Mawryngkneng and Lulung areas. The trend of the conglomerate is controlled by the trend of the quartzites and they are trending along NE-SW and dipping 50^0-60^0 towards NW direction (Map-1).

4.2.1.2 Current bedding

The current bedding of Mawryngkneng area is a common nondiastrophic structure observed in the quartzites. The internal bedding structures are mainly dominated by planar cross-stratification with truncated top and tangential bottom (Fig-4.2). This structure is diagnostic of the fluvial depositional regime of the time. Foreset beds of some units are essentially planes which are parallel to one another and meet the overlying (topset) and underlying normal bedding (bottomset) at a sharp angle. This type is generally known as angular current bedding (Photo-4.1a). Current bedded units in most places occur in successive sets which have been called grouped sets (Allen 1963) (Fig-4.2). Sometimes current bedding free bands slso observed between the current bedded quartzites (Photo-4.1d).

Photo-4.1d: Current bedding free band in current bedded quartzite exposed on the road sides at Mawryngkneng.

Structures produced by penecontempraneous deformation may also be observed in current bedded quartzites (Fig-4.3, Fig-4.4). The intensity of the penecontempraneous deformation was often so large that the foreset layers are deformed to isoclinal fold (Photo-4.2a). The development of convolute laminations indicate that both vertical and lateral movements may be associated in unconsolidated sediments (Photo-4.2b).

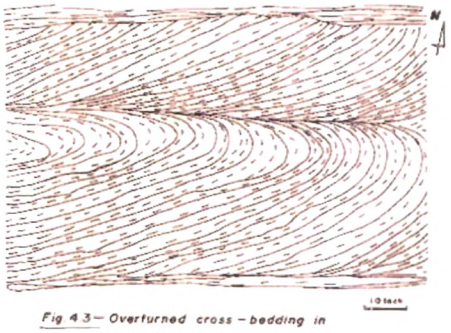

Fig 4.3 — Overturned cross-bedding in quartzites at Thangsalai.

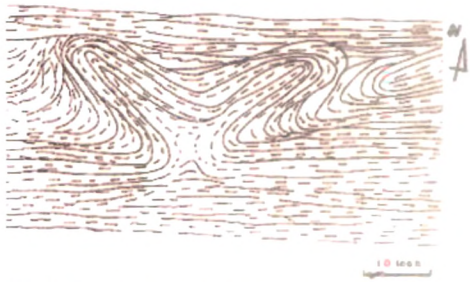

Fig 4.4 — Convolute lamination in quartzites at Ksehpongdeng road

Photo-4.2a: Overturned cross-lamination in quartzite on the valley at Thangshalai.

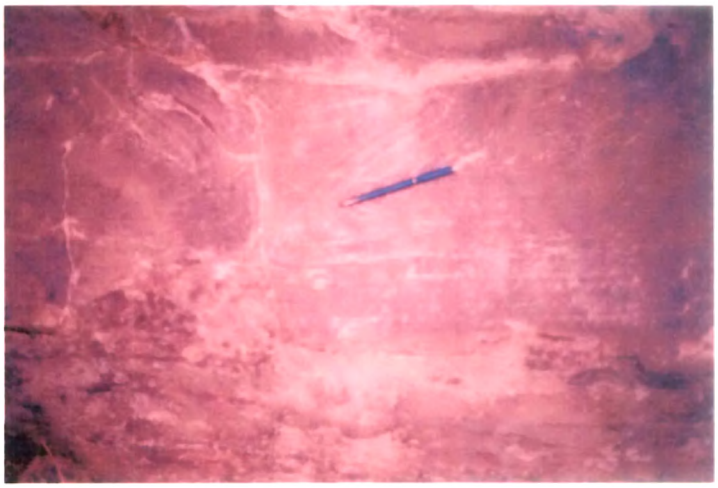

Photo-4.2b: Convolute lamination in quartzite on the Ksehpongdeng road.

4.2.1.3 Graded bedding

Graded bedding is best observed in Lulang conglomerate. The pebbles size varies from coarser at the bottom and relatively finer at the top of the conglomerate bed (Photo-4.2c). The size of the pebbles of the Nongplit conglomerate varies from 8 to 2.4 cm at the lower portion and 4 to 1.5 cm at

the top of the bed indicating a clear gradation in their size. Another depositional structure seen in the quartzites is a gradual increase in size of the sand grains towards the base of the bed, exhibiting graded bedding.

Photo-4.2c: Pebbles are comparatively finer towards northern part in the conglomerate at Lulung.

4.2.2 Linear structures

The primary linear structures (L_1) present in the rocks of the Shillong Group are ripple marks, oriented pebbles in conglomerate and parting lineation.

4.2.2.1 Ripple marks

Ripple marks are another depositional structures present in the quartzites of the Shillong Group. These marks are well preserved in the quartzites. Ripples are sinuous crested and have asymmetrical profile (Photo-4.3a). From the morphological study of the ripple marks of Mawryngkneng area the following results are found.

- Ripple index (RI) = 10.50
- Ripple symmetry index (RSI) = 3.20
- Parallelism index (PI) = 0.75
- Straightness index (SI) = 1.25

From the above morphological study it is clear that the ripples of the study area are current ripples and current direction indicated by the ripples towards south west.

The shape of the ripples provides a rough qualitative guide to flow velocity and water depth. Current ripples are most readily envisaged as forming in shallow water, but they are also produced in deep water due to the action of ocean bottom current (after Collinson and Thompson, 1989).

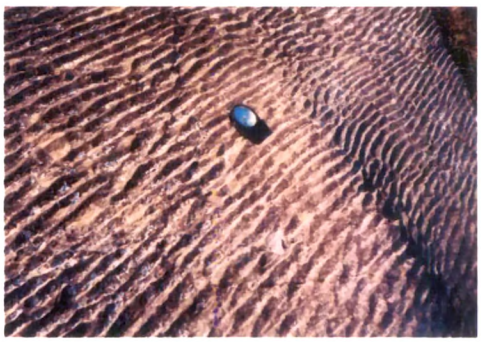

Photo-4.3a: Asymmetrical sinuous crested ripple marks in quartzite on the road side at Thangshalai.

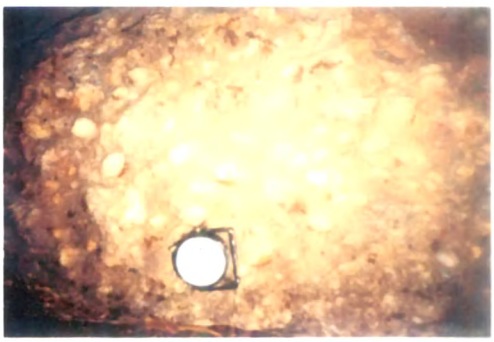

Photo-4.3b: Preferred orientation of long axes of the pebbles in conglomerates at Lulung.

4.2.2.2 Oriented pebbles in conglomerate

Conglomerate represents local break in deposition of sediments. The pebbles in the conglomerate beds are composed of quartzites and quartz, are elongate in shape and show a marked preferred orientation of their long (X)

axes (Photo-4.3b). All pebbles are highly cemented by siliceous, sericitic and fragments of quartz materials. The surfaces of the pebbles are smooth and lack angularity. This indicates that the pebbles have undergone prolonged fluviatile transportation. The trends of the long axes of the pebbles are NE-SW and maintain the same trend of bedding.

4.2.2.3 Parting lineation

This is a primary linear structure expressed as faint linear grains on bedding surfaces and records the current direction at the time of deposition of the sand grains. It is physically expressed as due to the subparallel alignment of the longest dimensions of sand or silt grains with bedding lamellae.

4.3 Palaeocurrent Analysis with the help of Nondiastrophic Structure

4.3.1 Introduction

Palaeocurrent analysis involves the study of ancient sediment dispersion patterns. As large bed-forms usually respond to a dominant flow and are not easily re-moulded by low-stage flows they tend to give a good indication of the palaeoslope.

The quartzites of the study area are characterized by ripple marks and current bedding and two beds of intraformational conglomerate are also encountered in the area. The regional trends of beds are NE-SW direction and dipping towards SE and NW directions ranging from 10^0 to 80^0.

4.3.2 Palaeocurrent analysis by rose diagram method

There are various methods for analysis of palaeocurrent. For the present study "Rose Diagram" method is followed.

4.3.2.1 Palaeocurrent from current bedding of quartzites

Current bedding is one of the most widely used palaeocurrent indicators. Current bedding of various shapes and sizes are the commonest tools used for palaeocurrent analysis. The reliability of different types of current bedding for palaeocurrent interpretation has been discussed by High and Picard (1974). For a planar-tabular cross-bedding, palaeocurrent is indicated by the direction of inclination of the foreset.

The current bedding in quartzites of Mawryngkneng area is of planar-tabular variety (Fig-4.5a). The internal bedding structures are mainly dominated by planar cross-stratification with truncated top and tangential bottom (Photo-4.3c). Such structures are diagnostic of the fluvial depositional regime of the time.

Photo-4.3c: Current bedding in quartzite with truncated top and tangential bottom at Shormo.

4.3.2.1.1 Field methods

The important attributes of a cross-bedded structure are its scale and its variability both in inclination and direction. Twelve locations at different localities of quartzites beds are taken for measuring data. At least 30 readings of dip and strike of the foreset beds are taken from each station. The most important measurements recorded in the field for current bedded strata for palaeocurrent analysis are the following:

- Dip and strike of the normal bedding.
- Dip and strike of the foreset beds.
- Thickness of the current bedded unit.
- Thickness of the topset, foreset and bottomset units.
- Length of the foreset beds.

4.3.2.1.2 Laboratory methods

As all the foreset beds are measured on tilted strata, they are corrected for bottomsets using stereographic net in the laboratory. For palaeocurrent analysis, classes are set up of the vector (0^0-360^0) into various classes at class intervals of 30^0. The various reading of the direction of inclination (bearing) noted from the various outcrops or stations are assigned to the various classes and the frequency percentage in each class determined (Table-4.1). The frequency percentages are calculated for each locality and histograms are prepared accordingly and azimuthal directions are determined (Fig-4.5b). The percentages of different classes are plotted in the "Rose Diagram", where the radius of the circle represents the percentage (Fig-4.5c). After completing the rose diagrams an arrow is marked against the maximum frequency. In case, there are two maxima, the arrow is put in between.

Table-4.1 : Frequency percentage of each vector class.

Station No.	180^0-209^0	210^0-239^0	240^0-269^0	270^0-299^0	300^0-329^0	330^0-359^0
1.	22	51	27	-	-	-
2.	8	45	30	17	-	-
3.	10	30	48	12	-	-
4.	20	50	30	-	-	-
5.	12	65	23	-	-	-
6.	6	40	40	14	-	-
7.	-	45	52	3	-	-
8.	-	47	47	6	-	-
9.	3	38	55	4	-	-
10.	-	35	58	7	-	-
11.	5	50	42	3	-	-
12.	3	42	54	1	-	-

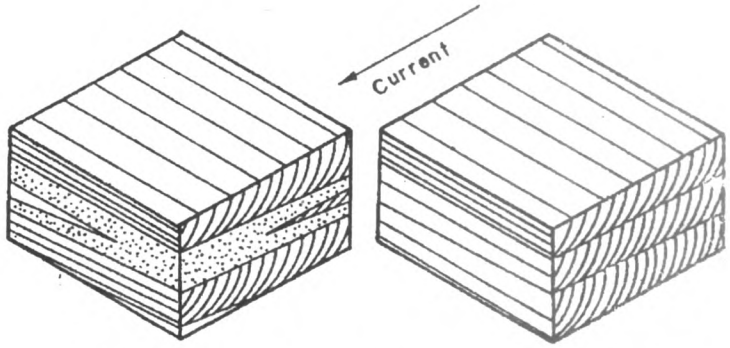

Fig-4.5a: Tangential current bedding in quartzite. Arrow indicates direction of current flow.

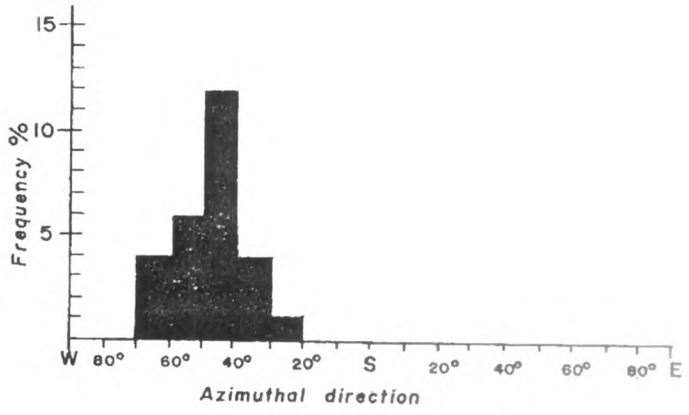

Fig-4.5b: Histogram of frequency percentage.

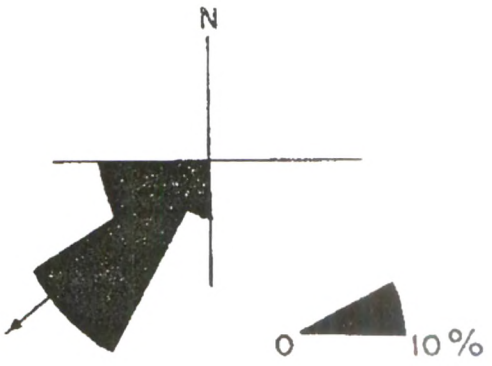

Fig-4.5c: Rose diagram showing current beddings azimuth.
Arrow indicates direction of current flow.

4.3.2.2 Palaeocurrent from pebbles of conglomerate

Two conglomerate beds are mapped in the Mawryngkneng area (Map.1). Geological observations indicate that long axes of the pebbles are oriented in the direction of current flow (White, 1952) or transverse to the same (Toenhofel, 1950). The present analysis revels that most of the pebbles are oriented along the current direction and a few are transverse to the former. The conglomerate is composed dominantly of quartzite pebbles and a few pebbles of quartz (Fig-4.6a). Pebbles free bands occurs in frequently through out the conglomerate bed and they are not sharply bounded by bedding planes and are distinguished by lake of pebbles (Photo-4.3d). In general, the pebbles are elongated oblate and well rounded.

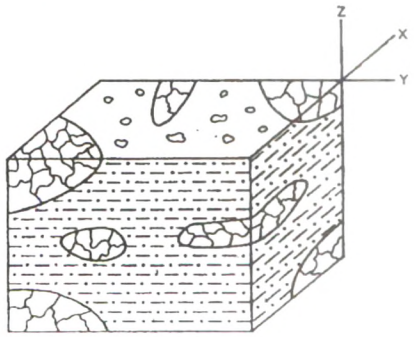

Fig-4.6a: Block diagram of conglomerate bed.

Photo-4.3d: Pebbles free band in conglomerate at Lulang.

4.3.2.2.1 Field methods

The three intercepts of the pebbles are made use of in calculating the mean size, flatness ratio, diameter, sphericity and shape factor. The azimuths of maximum intercepts are used in palaeocurrent study through vector analysis. In the field, the pebbles are so tightly packed that little tapping with hammer is necessary in some places to remove the pebbles. The three intercepts of the pebbles, maximum (X), intermediate (Y) and minimum (Z) have been measured in the field with the help of scale and slide caliper. Three stations are selected for collecting data from the conglomerate beds for measuring the intercepts of the pebbles and about 50 such pebbles are measured in each station. Before removing the pebbles from the beds, the azimuth direction and angle of inclination of the intercepts are measured with the help of clinometer compass.

4.3.2.2.2 Laboratory methods

The flatness ratios for individual pebbles are calculated from the formula X+Y/2Z (after Wentworth, 1922) and average is taken for each location. Shape factor XZ/Y^2 is calculated for individual pebbles and then mean value is taken for each location. From the intercepts the diameter'd' of the pebbles is

calculated using the formula $d=3\sqrt{XYZ}$. Sphericity is calculated from the formula d/X (Table-4.2).

Table No-4.2 : Summary of analysis of conglomerate pebbles.

Location No.	Diameter in cm.	Flatness ratio	Sphericity	Shape factor
1	1.00	2.80	0.58	0.70
2	2.56	3.15	0.48	0.89
3	1.20	2.75	0.60	0.71

The conglomerate beds in the field show high inclination, so the pebbles do not give true picture of the original azimuth and inclination of the long axes at the time of deposition. In order to determine their original attitudes, the axes are rotted about the strike of the enclosing beds following the method of structural tilt problem. The angle of inclination of the long axes (X) of pebbles of all the stations are combined and grouped into 10^0 intervals and a histogram is prepared with the frequency percentage (Fig-4.6b). All the azimuthal data of X-axes are grouped into 30^0 intervals, frequency percentage are calculated and shown in a Rose Diagram (Fig-4.6c).

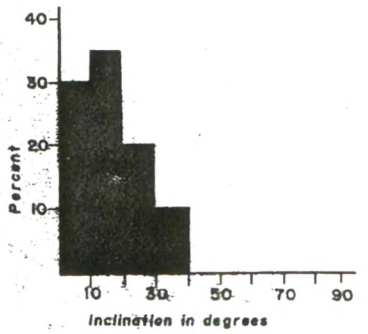

Fig-4.6b: Histogram showing pebbles inclination with the conglomerate bed.

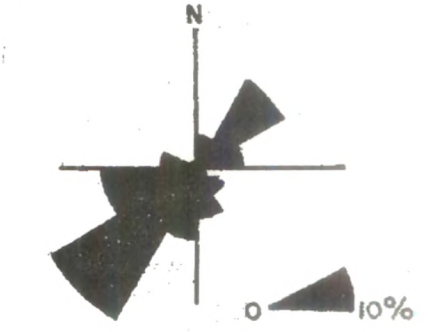

Fig-4.6c: Rose diagram showing azimuthal distribution of long axes (X).

4.3.3 Palaeocurrent map

In the study area, total 15 stations are selected for palaeocurrent current analysis. After completing the rose diagrams for every stations an arrow is marked against the maximum frequency. In case, there are two maxima, the arrow is put in between. The prepared rose diagrams are then plotted at the respective stations or outcrop with the arrow mark on the base map, which reveals the palaeocurrent direction. The map prepared by plotting the rose diagrams in their respective stations is called the palaeocurrent map(Fig-4.6d).

The palaeocurrent analysis reveals that the current direction in the sediments of the Shillong Group of rocks was from NE to SW at the time of deposition. The pebbles are of high sphericity indicating that they have been transported to longer distance i.e. provenance was found far away from the depositional site.

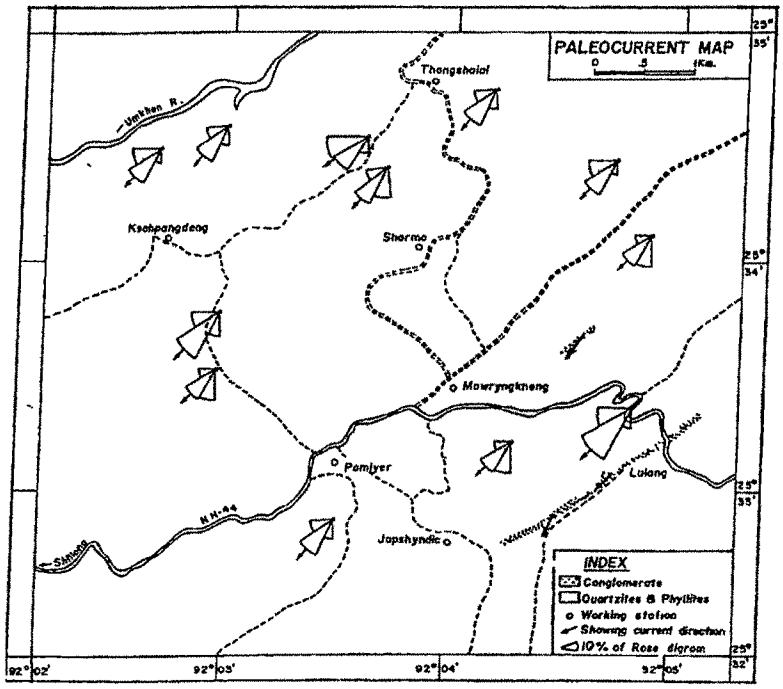

. **Fig-4.6d:** Palaeocurrent map of the study area

4.4 Diastrophic structures (Secondary)

The upper part of the Shillong Group of rocks of Mawryngkneng area is highly deformed and metamorphosed as a result of which the original rocks are transformed into quartzites, phyllites and conglomerates. The general trend of the foliation is NE-SW direction. Various planar structures like continuous and space cleavages as well as linear structures are marked by elongated pebbles of conglomerate, fold axes, intersection and mineral lineation and corresponding folds of different generations. These are the important structures of the area. The variety of secondary structures observed in the rocks can be broadly classified as planar and linear structures.

4.4.1 Planar structures

The secondary planar structures developed in the rocks of the area generally include various foliations, joints, quartz veins, etc.

4.4.1.1 Foliation (S_1)

The S_1 is comprised of a set of cleavage that lies parallel to the bedding or lithological layering (S_0). Slaty cleavage developed in fine grained phyllite is characterized by parallel arrangement of platy minerals such as sericite, chlorite, muscovite and ellipsoidal grains of quartz (Photo-4.4a). Because of this probably the phyllite is cleared into perfectly tabular thin plates or sheets (Photo-4.4b). In the quartzites, this type of planar structures is rare, but where present is marked by elongate and flattened quartz grains. This cleavage strikes along NE-SW and dipping towards NW and SE directions with varying angles from 50^0 to 90^0. The foliation S_1 run parallel to the lithological layering S_0 (Fig-4.7).

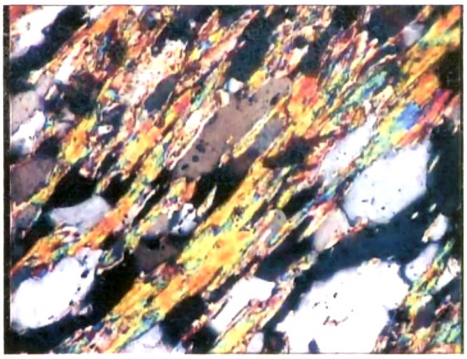

Photo-4.4a: Parallel arrangement of platy minerals in quartzite. Cross polars x10. Locality: Mawryngkneng.

Photo-4.4b: Tabular thin plates or sheets developed due to slaty cleavage in phyllite at Mawryngkneng near petrol pump.

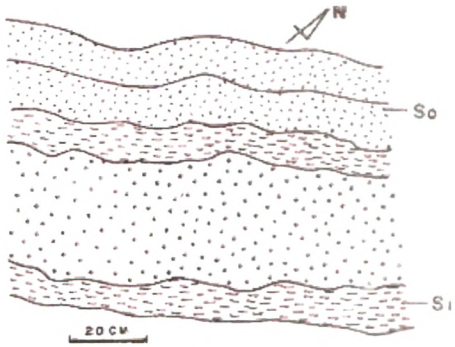

Fig-4.7: Lithological layering S_0 in quartzites and dominant foliation S_1 in phyllites. Locality: Shormo

4.4.1.2 Foliation (S_2)

This set of cleavage is axial planar to the F_2 folds and are also penetrative in nature. The S_2 is marked by the parallel alignment of micaceous minerals in the pelitic rocks of the area. The axial plane of crenulations and minor open folds represent S_2 cleavage intersecting S_1 foliation at a very high angle (Fig-4.8, Fig-4.9) (Photo-4.4c, Photo-4.4d). S_2 cleavage is clearly distinguished from S_1 in case of critically refolded exposures maintaining occasional coaxiality by cross cutting relationship where S_1 is folded by F_2 and S_2 cut the S_1. S_2 is also defined by the growth and accumulation of mica minerals along the strain zones of F_2 folds (Photo-4.5a).

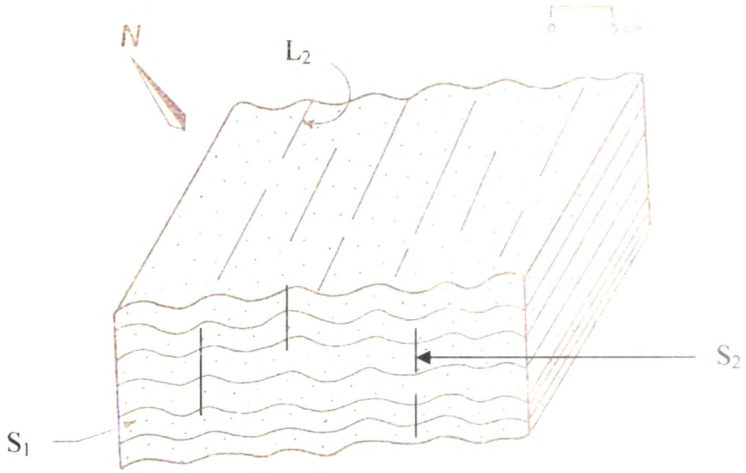

Fig-4.8: Crinkle cleavage in phyllite at Pamlyer (Ksehpongdeng road). Axes of the crenulation are the L_2.

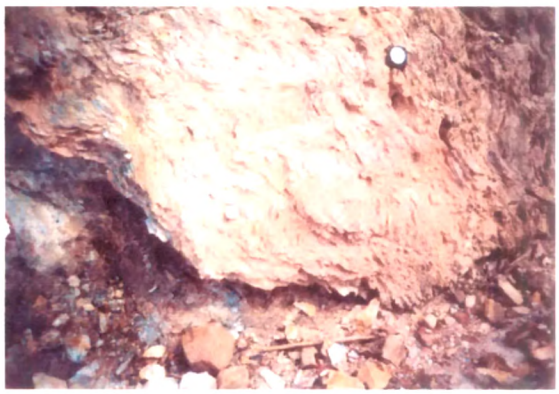

Photo-4.4c: Crinkles (crenulation cleavage) developed in phyllites at Pamlyer Ksehpongdeng road.

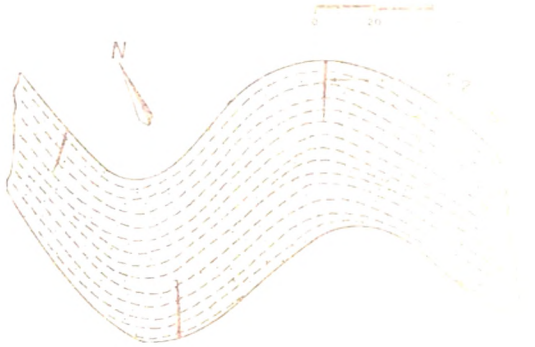

Fig-4.9: Minor open fold in phyllite at Japshyndit hillock, Mawryngkneng.

Photo-4.4d: Gently plunging minor open fold in phyllite at Japshyndit hillock. Mawryngkneng

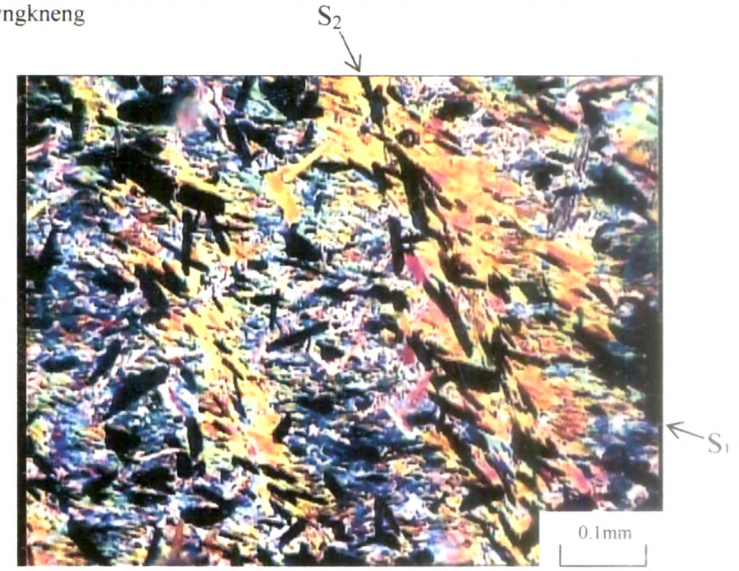

Photo-4.5a: Accumulation of mica minerals along the strain zones of F_2 fold. Cross polars x10. Locality: Ksehpongdeng road.

4.4.1.3 Foliation (S_3)

Cleavages parallel to the axial planes of the F3 folds are designated as S_3. The generalized trends of the foliation are NE-SW direction with gentle plunge towards NE.

4.4.1.4 Joints

Joints are well developed in quartzites. They are also developed in phyllites and conglomerates. Besides these joints are also observed in amphibolites and granites. Maximum measurements of joints are taken from quartzites and phyllites of the area. Most of the joints are longitudinal joints, cross joints and oblique joints (Fig-4.10). Hence, they form the rocks into rectangular blocks (Photo-4.5b.

Fig-4.10: Block diagram showing the development of various sets of joint in the Shillong Group and their relation to fold closures.

Photo-4.5b: Joints developed in quartzites of Shillong Group.
Locality: - Near Puriang.

The abundance of jointing at a station where joints are well developed is described through the evaluation of joint density. A circle is made with

diameter of 2 meters on a bedrock surface of perfectly exposed jointed rock at Ksehpangdeng near water pump. Then orientation and trace length of each fracture within the circle are measured. Joint density with the circle inventory method is the summed length of all joints within the inventory circle divided by area of the circle is represented by an equation $P_j = L/\pi r^2$(Davis 1984, p.343).

Where, **Pj**= Joint density
L = Cumulative length of all joints
r = Radius of inventory circle

The joint density is expressed in units of length/area (cm/cm^2). Fracture density is shown in the table below (Table-4.3).

Locality:- Ksehpangdeng near water pump
Circle is made on quartzites rock
Radius of inventory circle = 100cm.
Area = 31428 cm^2

Table: 4.3 Fracture Density

Trend of fracture	*Length of fracture (in cm.)*	*Trend of fracture*	*Length of fracture (in cm.)*
N40E	200	N38E	200
N20W	125	N25W	50
EW	200	N33W	200
N31W	192	N40W	120
N25E	200	N50W	70
N29E	170	N45E	130
N22W	200	N32W	200
N35W	90	N55W	80
N20E	182	N10W	80
N25E	150	N46E	160
N50E	200	N35W	200
N45E	50	N30W	82
N45W	105	N15W	90

Cumulative fracture length = 3726

[Fracture density = 3726 cm/31428 cm^2 = 0.12 cm^{-1}]

The orientation data of joints collected in the field are analyzed in the laboratory with the preparation of contour diagrams, rose diagrams and strike histograms.

About 450 joints reading have been taken from Ksehpangdeng, Thangshalai, Mawryngkneng and Puring areas (Table-4.4). These joints were plotted in Schmidt equal area net and were later contoured with the methods given by Turner and Weiss (1963). The contour diagrams reveal the presence of three sets of joints. The pattern of orientation of joints varies from diagram to diagram i.e. locality to locality (Fig-4.11). The most important sets of joints are the longitudinal joints, cross joints and oblique joints (Table-4.4).

Table 4.4 : Description of the contour diagrams.

Serial No.	*Locality*	*No. of Readings*	*Attitude of Foliation*	*Sets of joints*	*Fig. No. 4.11*
1.	Ksehpangdeng	100	55/70 SE	1. $N50^0W$-$S50^0E$	
				2. $N40^0E$-$S40^0W$	(a)
				3. $N80^0W$-$S80^0E$	
2.	Thangshalai	100	50/65 SE	1. $N60^0W$-$S60^0E$	
				2. $N45^0E$-$S45^0W$	(b)
				3. $N85^0E$-$S85^0W$	
3.	Mawryngkneng	150	235/60 NW	1. $N45^0W$-$S45^0E$	
				2. $N30^0E$-$S30^0W$	(c)
				3. $N10^0W$-$S10^0E$	
4.	Puring	100	230/65 NW	1. $N35^0W$-$S35^0E$	
				2. $N60^0E$-$S60^0W$	(d)
				3. $N5^0W$-$S5^0E$	

Index: - 1. Cross joints 2. Longitudinal joints 3. Oblique joints

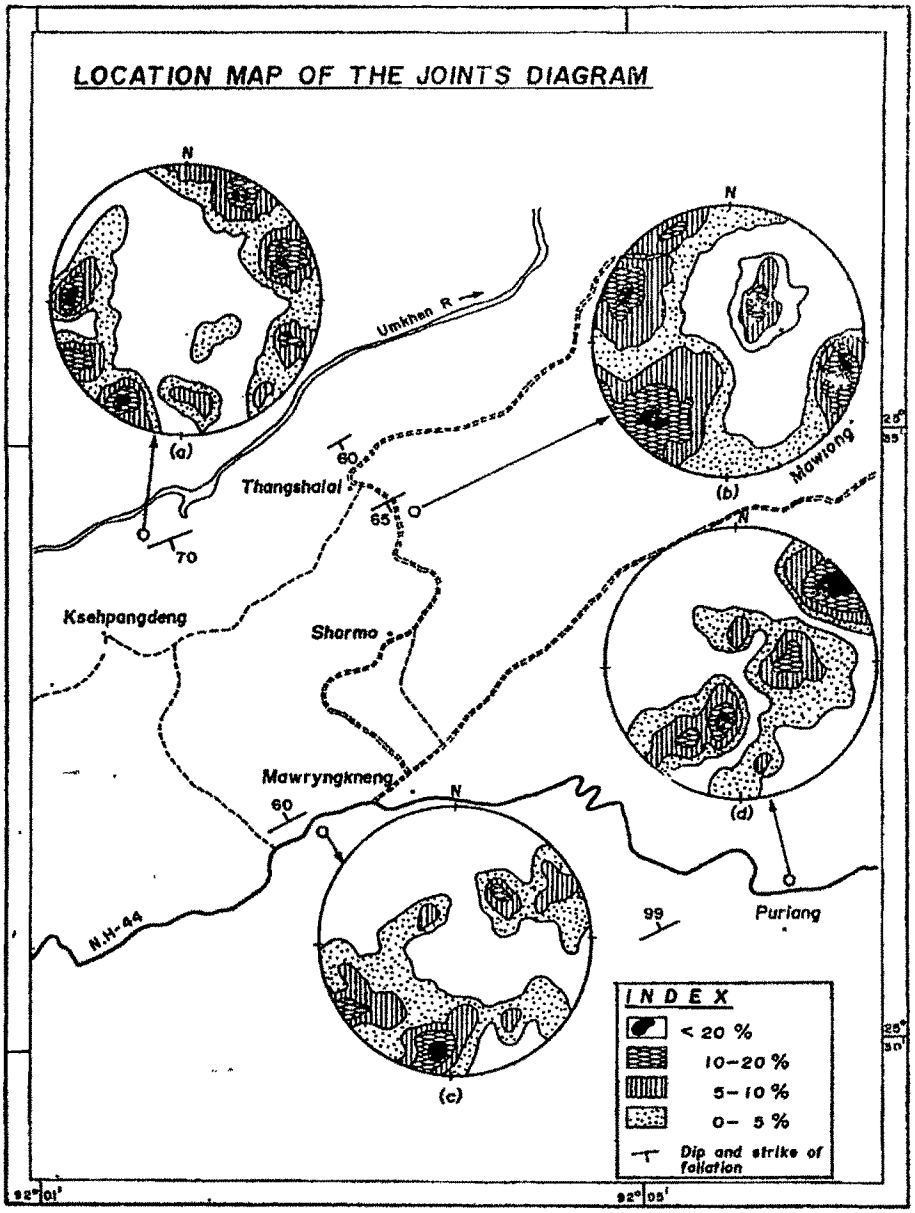
LOCATION MAP OF THE JOINTS DIAGRAM
N
(a)
Umkhen R
Thangshalai
60
65
70
(b)
Mawlong
Ksehpangdeng
Shermo
Mawryngkneng
60
(c)
(d)
99
Puriang
N.H-44
INDEX
< 20 %
10-20 %
5-10 %
0- 5 %
Dip and strike of foliation
92°01'
92°05'
25°
25°30'

Fig-4.11

Strike histograms are prepared with the strike data of Ksehpangdeng, Puring and Mawryngkneng area. Data are first arranged into class intervals of 10^0, encompassing the orientation range from west through north to west. The number and percentage of readings that fall within each class interval are then counted. The class intervals are plotted along the Y axis and the numbers of readings are plotted along the X axis of an X-Y plot. From the strike histograms it is clear that the cross joints are prominent one (Fig-4.12a, b, c).

Rose diagrams have been prepared with the trend (strike) data. For rose diagrams, class intervals are taken as arc of 10^0. Three rose diagrams are prepared from the data collected from Ksehpangdeng, Puring and Mawryngkneng areas (Fig-4.13a, b, and c).

From the above contour diagrams, rose diagrams and strike histograms it is clear that the joints are the longitudinal joints, cross joints and oblique joints. The cross joints are the dominant set followed by oblique set and by the longitudinal set. This indicates that the rocks are fractured more across and least along the foliation of the rocks. It is obvious that the pattern of orientation of joints varies from place to place. At Ksehpangdeng and Mawryngkneng the cross and oblique joints are more prominent than the longitudinal set, while at Puring the oblique and longitudinal sets are least and cross joints are dominant. From the joint orientation diagrams it is clear that the principal compressive stress in NW-SE direction.

The presence of these joints in the rocks, indicates that they were ductile developed after the deformation and associated metamorphism and are the end products of brittle deformation.

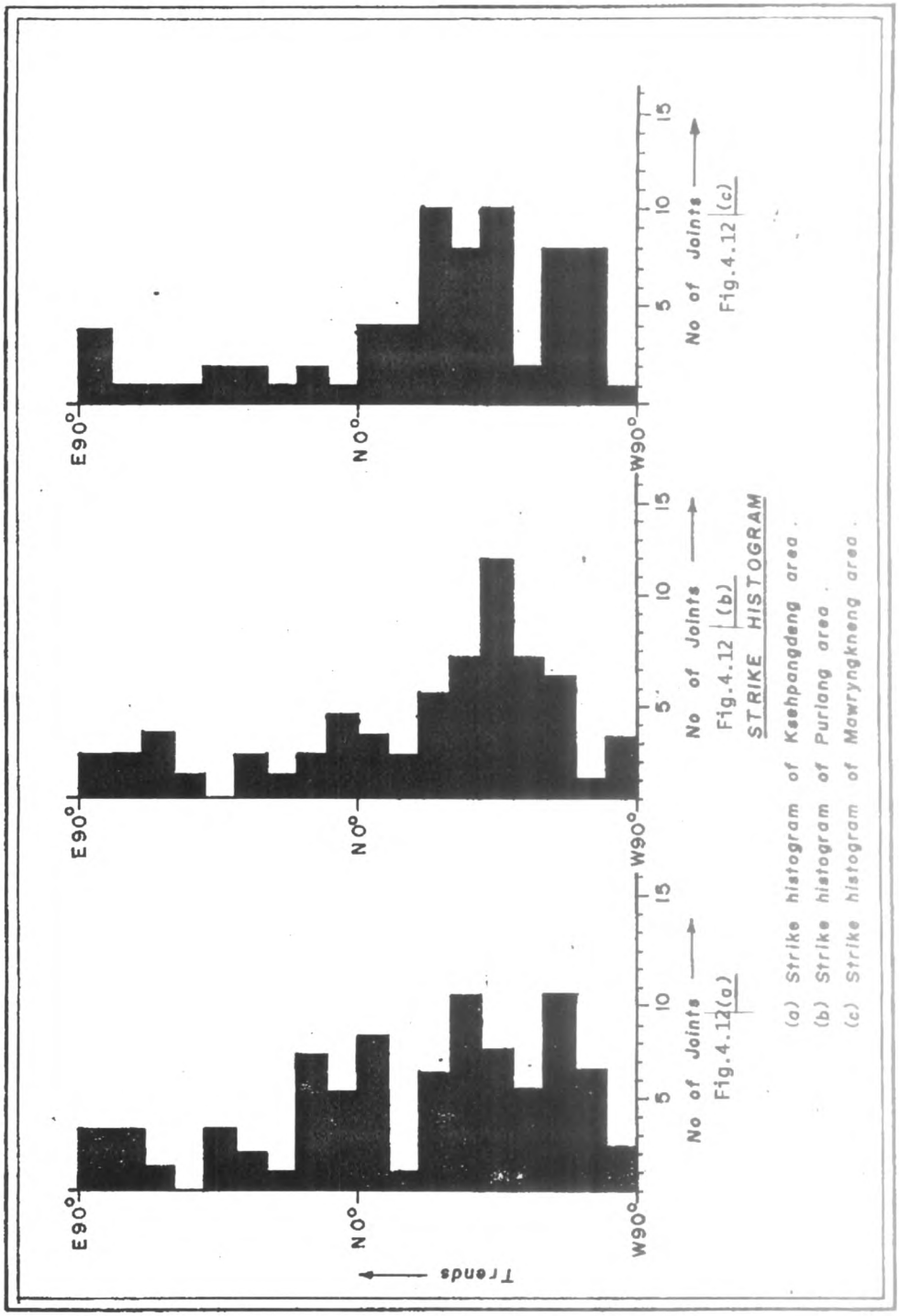
E90°
N0°
W90°
Trends
No of Joints
5
10
15
Fig.4.12(a)
Fig.4.12 (b)
Fig.4.12 (c)
STRIKE HISTOGRAM
(a) Strike histogram of Kashpangdeng area.
(b) Strike histogram of Purlang area.
(c) Strike histogram of Mawryngkneng area.

Fig-4.12

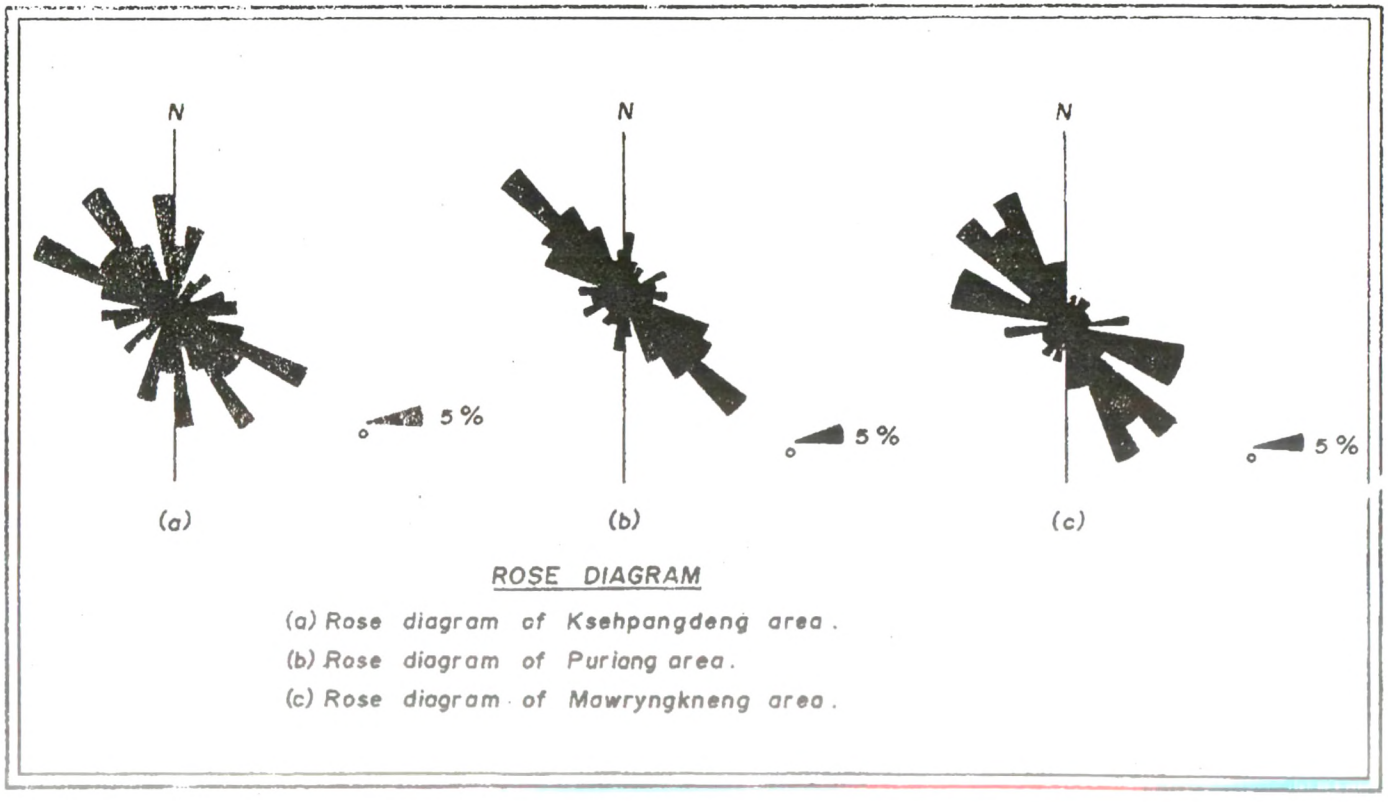

ROSE DIAGRAM

(a) Rose diagram of Ksehpangdeng area.
(b) Rose diagram of Puriang area.
(c) Rose diagram of Mawryngkneng area.

Fig-4.13

4.4.1.5 Quartz veins

The rocks of Shillong Group are criss-crossed by quartz veins (Fig-4.14). Quartz veins in various dimension occur in quartzites are well exposed in the study area. The thickness of the veins ranges from about 1cm to 30cm. Two sets of veins, one set of vein parallel to foliation planes and other set across the foliation are well developed in the rocks of the study area (Fig-4.15a, Fig-4.15b, Photo-4.5c and Photo-4.6a).

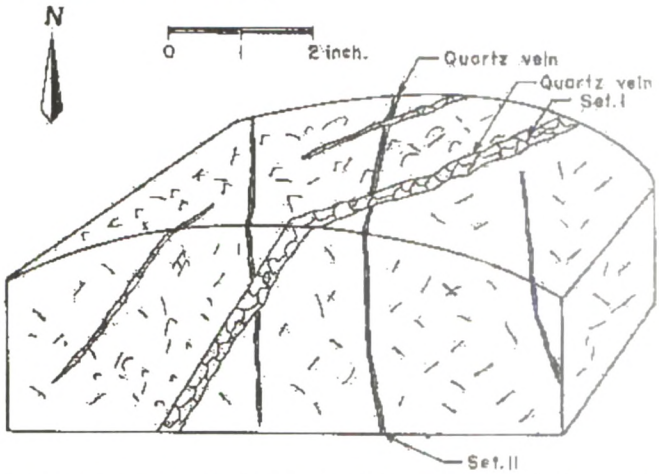

Fig-4.14: diagram showing the dominant type of quartz vein in quartzite.

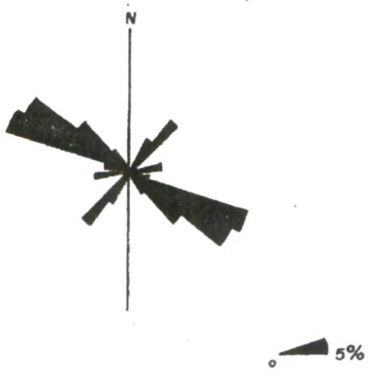

Fig.4.15a Rose showing trend of quartz vein

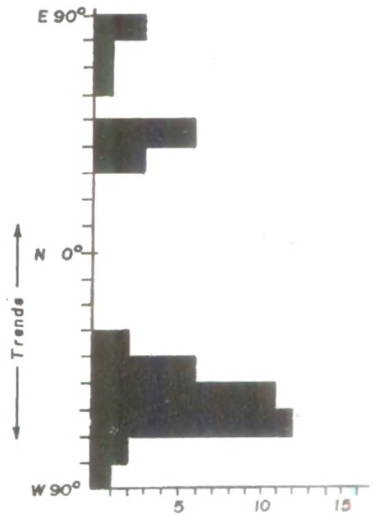

Fig.4.15b Bar shiwing trend of quartz vein

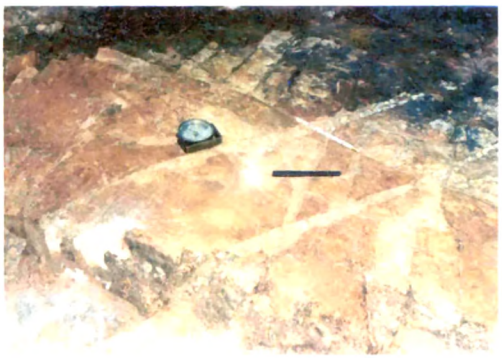

Photo-4.5c: Quartz vein developed across the foliation in quartzites at Ksehpongdeng

Photo-4.6a: Quartz vein developed along the foliation in quartzites at Pamura.

4.4.2 Linear Structures

Various types of linear structures are present in the rock of the investigated area. Linear structures are developed due to the deformation and associated metamorphism of the Shillong Group of rocks. The main types of lineation are stretched pebbles of conglomerate, mineral lineation, intersection lineation and fold axes lineation. These are denoted here as L_1, L_2 and L_3.

4.4.2.1 Lineation (L_1)

This lineation is best represented by the original lineation, pebble lineation, intersection lineation coinciding with the attitude of the F_1 fold axes. The long axes of the pebbles in conglomerate are nearly parallel to one another Mineral lineation is marked by the preferred orientation of quartz, mica flakes and chlorite minerals (Photo-4.6b). The micaceous platy minerals like muscovites and chlorites have grown due to metamorphism and this mineral growth in such a way that these platy minerals have their long dimension parallel to each other (Photo-4.6c). This mineral lineation generally parallel to the trend of the S_1 foliation, hence usually NE-SW and they plunge at varying angles ranging from 20^0 to 40^0 towards either to NE or to SW.

Photo-4.6b: Mineral lineation in quartzites at Puriang.

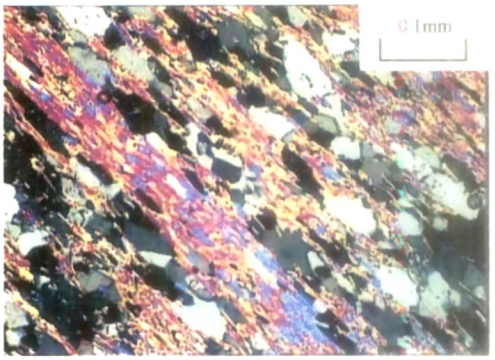

Photo-4.6c: Mineral lineation shown by parallel arrangement of mineral in mica schist at Mawryngkneng. Cross polars x10

4.4.2.2 Lineation (L_2)

This lineation is marked by the axes of F_2 crenulations, intersections of S_1 and S_2 (Fig-4.8, Photo-4.4c). The micaceous platy minerals forming cleavage domain generally parallels in phyllites and such domains are axial planar to F_2 fold (Photo-4.5a).

4.4.2.3 Lineation (L_3)

Lineation L_3 developed due to intersection lineation of S_3 cleavage with the pre-existing set of cleavage and slickensides. Slickensides are perpendicular to the strike of the rocks indicating their development due to slip along the dip of the beds (Fig-4.16).

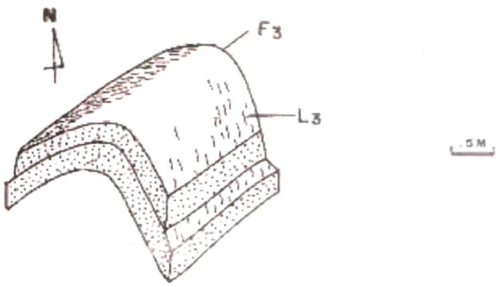

Fig-4.16 *Open fold in quartzites, Slikensides are developed along the dip direction of the F3 fold. Locality — Thangsalai*

4.4.3 Folds

In the area under investigation folds are very common structural features. The sizes of the folds are from microscopic scale to macroscopic scale. Folds measuring from a few centimeters to kilometers are found in the Shillong Group of rocks. It may be mentioned here that the designation of folds as F_1, F_2 and F_3 is comparative and is based on the correspondence of folds in the tectonic units. For the analysis of the major fold structure, the area map has been divided into 5(five) domains and the stereographic plots of various structures are shown in map (Map.2).

4.4.3.1 Folds (F_1)

F_1 fold are present only on the phyllites of the Shillong Group. They are small, tight isoclinal folds (Fig-4.17, Photo-4.6d). The wave length of these minor fold ranges from 3cm to as much as 1m.

The F_1 folds are accompanied by strong axial-plane schistosity S_1 suggesting that the metamorphism was synchronous with the deformation F_1. The fanning of this schistosity is slightly convergent in the direction opposite to the fold closures and further suggests that the schistosity developed in the later stages of folding. The axial planes of the F_1 folds are sub vertical (Fig-4.17, Photo-4.6d). The trend of the axial planes is NE-SW, dipping towards NW. The orthogonal thickness of the layer always has a minimum value on the flank of the fold and a maximum value at the hinge of the fold. Hence, folds shape varies from class 1C to 2 (Ramsay, 1967).

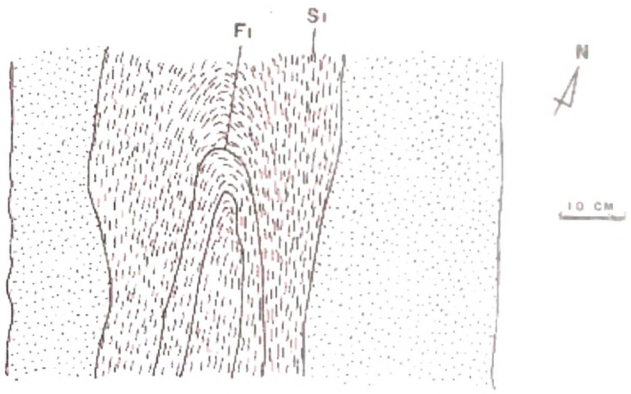

Fig-4.17: *An isoclinal F1 fold in phyllites of Shillong group. Locality — Puriang*

Photo-4.6d: Isoclinal fold in phyllites of Shillong Group. Locality:- Puriang.

4.4.3.2 Folds (F_2)

F_2 folds are minor open folds developed almost at right angle to the F_1 folds. The interlimb angle of the F_2 folds are varies from 70^0 to 110^0. The orthogonal thickness of these folds shows slightly maximum at the hinge position and therefore belongs to class 1B and 1C type (Ramsay, 1967). These folds have a rectilinear hinge line parallel to the fold axis hence F_2 folds are plane cylindrical folds. The axes of F_2 folds are co-axially superimposed over F_1

folds (Fig-4.18, Photo-4.7a). The axial surfaces have a mean NE-SW trend and fold axes show a gently plunging towards SW (Fig-4.20a, Fig-4.20b, Photo-4.4d). F_2 folds are also associated with the crenulation cleavage S_2 (Photo-4.4c). Crinkles developed in phyllite are encountered at the road cutting near Pamlyer (Ksehpangdeng road). These are developed due to the puckering of the S_1. The axes of the crinkles are the L_2 lineation of the rocks (Fig-4.8, Photo-4.4c).

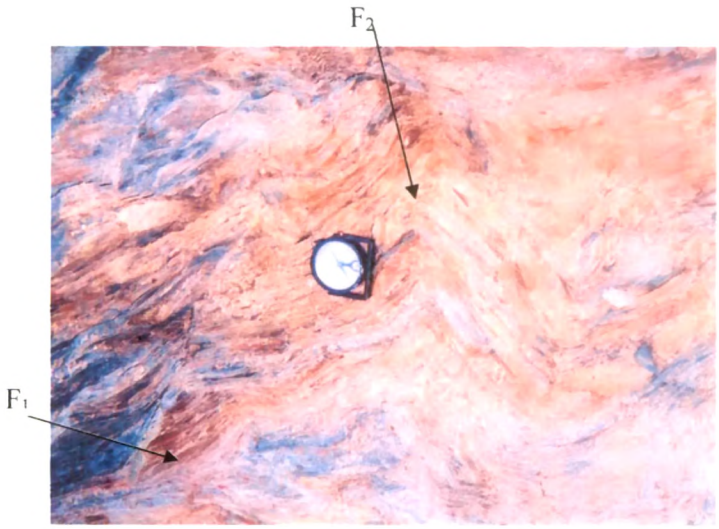

Photo-4.7a: F_2 fold in phyllite of the Shillong Group at right angle to F_1 fold. Locality:- Puriang

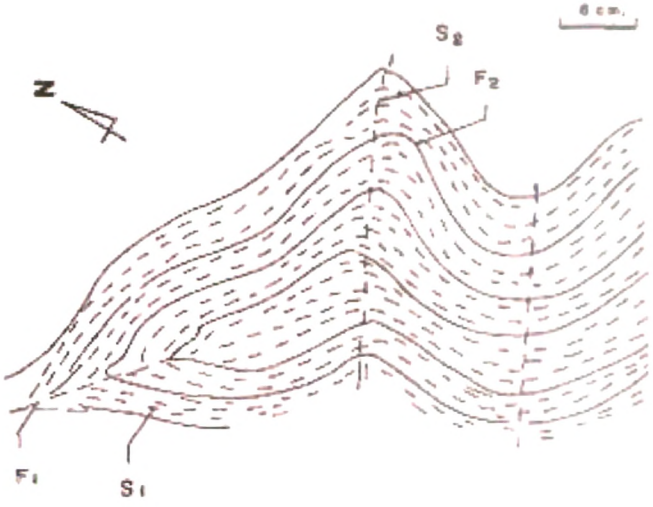

Fig-4.18: F_1 fold refolded by open F_2 fold in phyllites of Shillong Group at Puriang.

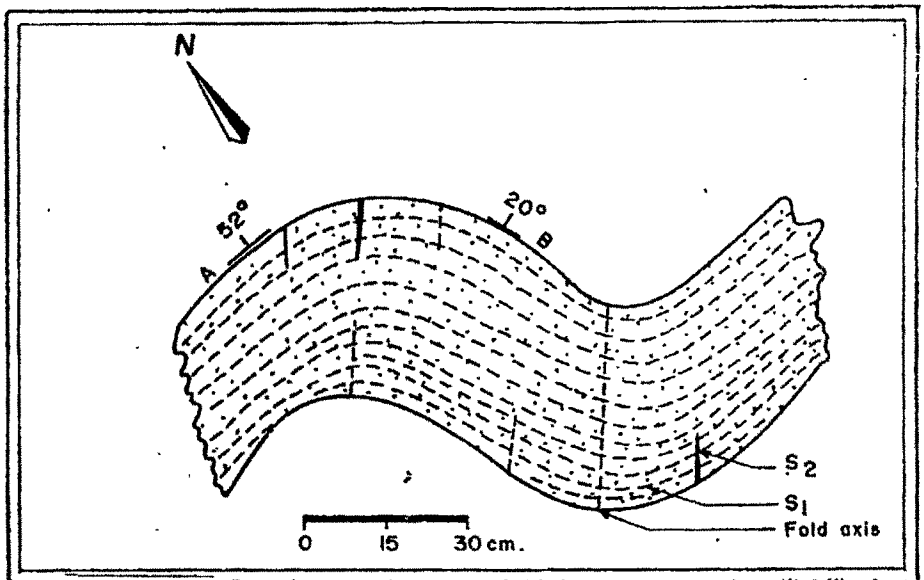

Fig.4.20a- *Phyllite showing open fold found at Japshyndit hillock (Oriented at field).*

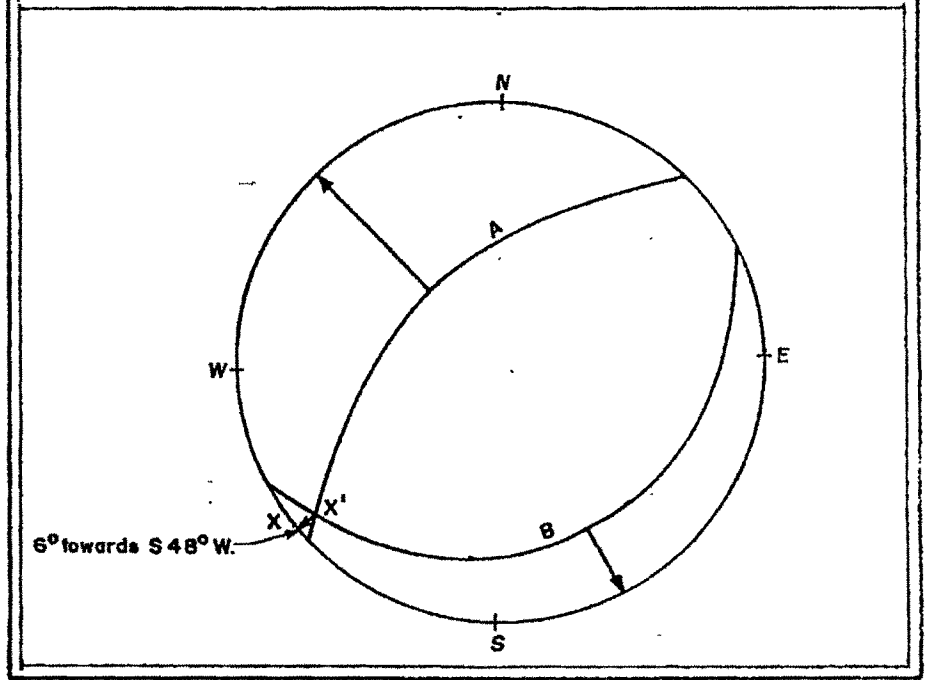

Fig.4.20b *Projection diagram of open fold. Fold axis X-X', plunges 6° towards S 48° W. Pitch on A-7°, B-15°.*

4.4.3.3 Folds (F_3)

The F3 folds belong to the last phase of folding history of the area and are well developed in the whole area and are superimposed over the older structures. They have varied geometric shapes, size and orientations over the area. Commonly they are open having steeply inclined axial surfaces. In style they are symmetrical fold and belong to class 1B of Ramsay (1967).

The kink bands, kink folds and conjugate folds are developed in the laminated phyllites, which show fine planar anisotropy (Fig-4.19a, Fig-4.19b, Photo-4.7b, Photo-4.8a and Photo-4.8b). The kink planes (axial plane) are moderately inclined and fold axes have plunges 10^0 to 20^0 towards SW direction.

The open folds of both symmetrical and asymmetrical in nature are found in the quartzites, which are produced by a flexural-slip mechanism due to which pre-existing quartz veins get separated along the slip-planes, and each part of the quartz veins moved up-dip with respect to the other part (Fig-4.16, Photo-4.8c, and Photo-4.8d).

Photo-4.7b: Kink developed in phyllites of the Shillong Group at Puriang.

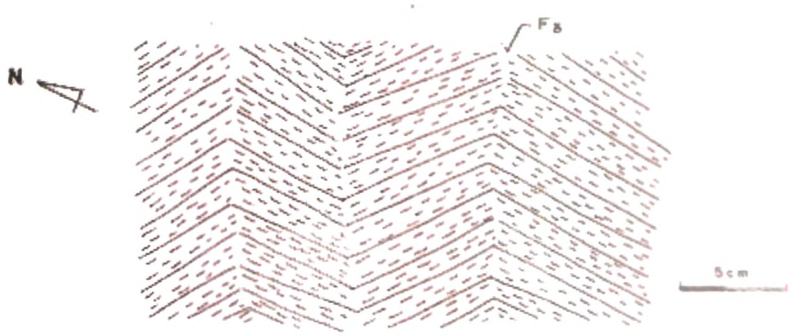

Fig. 4.19 (a) — Chevron fold developed in phyllites of Shillong group. Locality — Puriang.

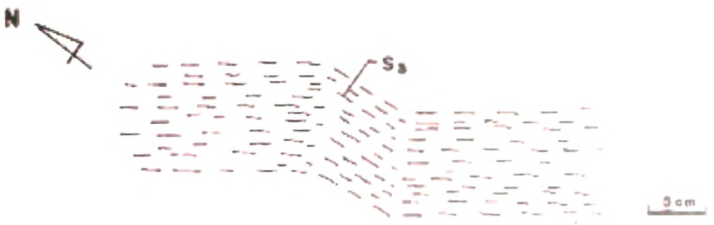

Fig. 4.19 (b) — Kinking in phyllites. Locality — Puriang.

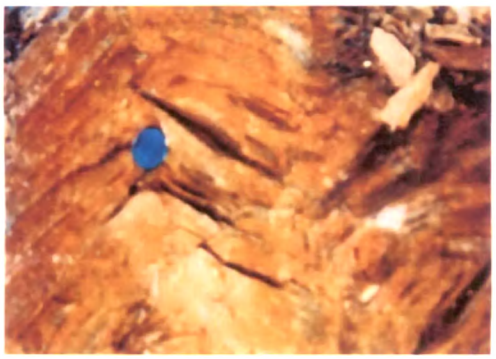

Photo-4.8a: Chevron fold developed in phyllites at Puriang

Photo-4.8b: Conjugate kink developed in phyllites at Puriang

Photo-4.8c: Open F_3 fold in quartzites of Shillong Group at Thangshalai.

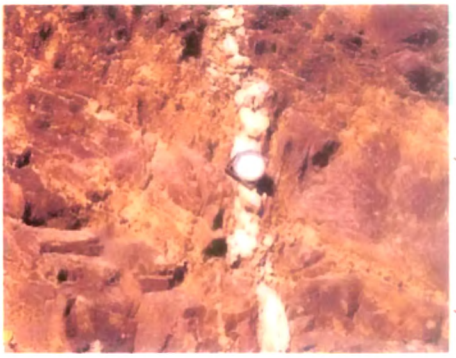

Photo-4.8d: Flexural slip folding has segmented the quartz vein, where upper segment has moved updip relative to the lower segment at Thangshalai.

Over and above these folds, the existence of major F_3 fold is revealed by the repetition of rock units, attitude of bedding or foliation and strongly developed minor F_3 folds (Map-1). When one goes from Mawryngkneng to Puriang he will find dipping of beds towards NW, and from Mawryngkneng to Ksehpangdeng it is towards SE direction. The presence of this fold (synform) is also evident from the section of the map (Map-1). This synclinal structure is identified as the F_3 fold. To determined the orientation of the major fold, the lithological layering S_0 are measured at various stations in the study area and whole area is divided into 5(five) domains for this purpose (Map-2).

In domain I, at Mawiong and Thangshalai distribution of S_0 poles indicate the trends of the foliation in NE-SW and S_0 dip at moderate angles towards SE (Fig-4.21).

In domain II, at Lumkyathang a bi-model distribution of S_0 poles is found, where the S_0 dip towards the NW at high angles and towards SE at moderate angles (Fig-4.22). The fold axis plunges towards $N45^0E$ at an angle of 8^0. The axial plane of the fold dips 80^0 towards NW direction.

In domain III, at Ksehpangdeng and Pamlyer also a bi-model distribution of S_0 poles is found, where the S_0 dip towards the NW and SE at high angles (Fig-4.23). The fold axis plunges towards N41^{0}E at an angle of 4^0. The axial plane of the fold dips approxjmately85^0 towards NW direction.

In domain IV, at Mawryngkneng and Shormo also a bi-model distribution of S_0 poles is found, where the S_0 dip towards the NW and SE at high angles (Fig-4.24). The fold axis plunges towards N43^{0}E at an angle of 7^0. The axial plane of the fold dips approximately 85^0 towards NW direction.

In domain V, at Nongplit and Puring distribution of S_0 poles indicate the trends of the foliation in NE-SW and S_0 dip at moderate angles towards NW direction (Fig-4.25).

The repetition of beds in the study area is due to the major F_3 fold (Mawryngkneng synform). This is a sub horizontal fold have plunge 4^0 to 8^0 towards NE. This major fold is an open fold. The mean attitudes of dip of bedding are at 70^0 towards N60^{0}W and 60^0 towards S37^{0}E.

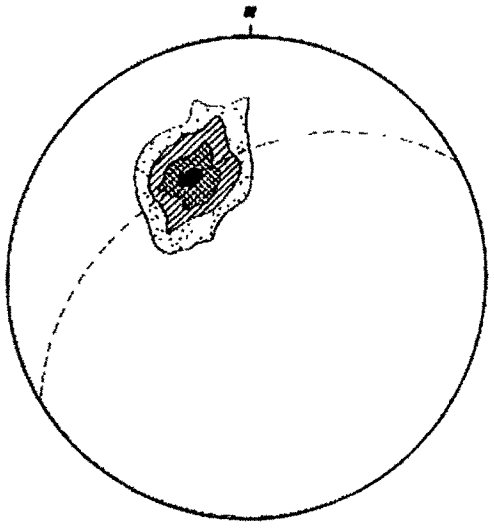

Fig. 4.21 — Contoured stereogram of 100 poles to foliation (So) from domain I (Thangshalai & Mawlong)

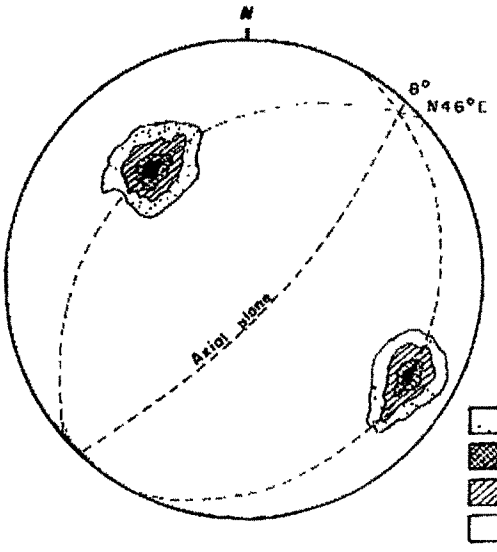

Fig 4.22 — Contoured stereogram of 100 poles to foliation (So) from domain II (Lumkyathang)

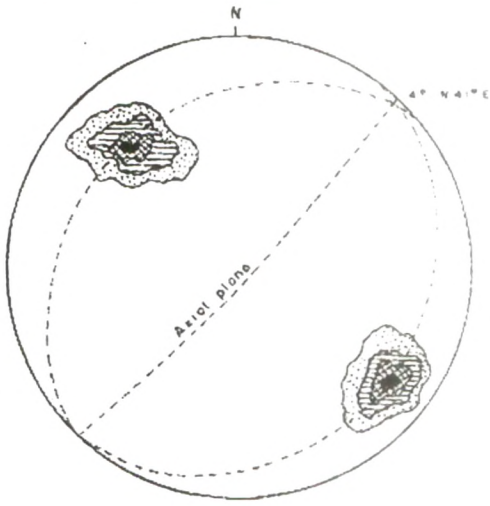

Fig. 4.23 — Contoured stereogram of 100 poles to foliation So from domain III (Ksehpangdeng and Pamlyer.)

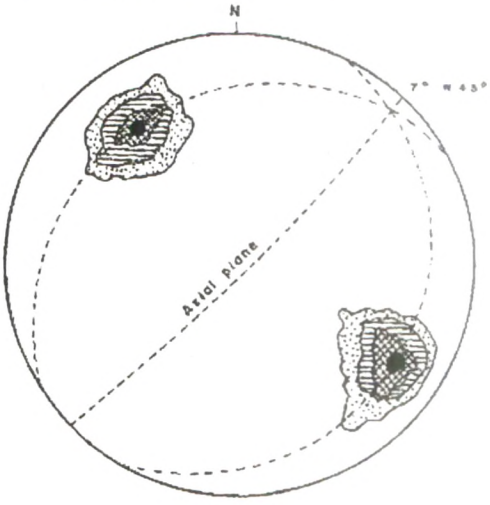

Fig. 4.24 — Contoured stereogram of 100 poles to foliation S_0 from domain IV (Mawryngkneng and Shormo.)

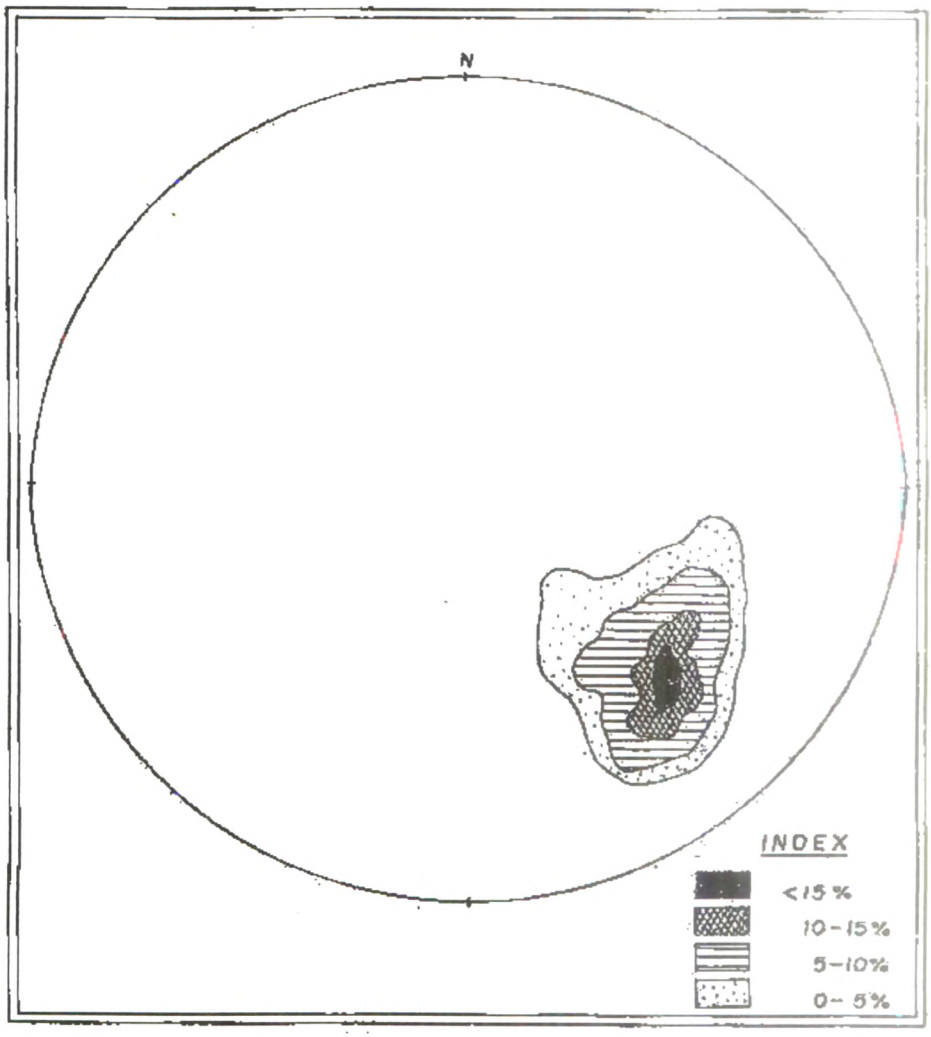

Fig-4.25: Contoured stereogram of 60 poles to foliation S_0 from domain V (Nongplit and Puriang)

4.5 Strain Analysis of Deformed Pebbles from Conglomerate

4.5.1 Introduction

Two conglomerates beds are well exposed in and around the Mawryngkneng area. One is developed 500m away from the weekly market towards east near grave yard. The average thickness of this bed is about 4m and striking in the NE-SW direction, with high angle of dip 55^0 to 85^0 generally towards NW. Pebble-free bands also observed within the conglomerate bed which is ranging often up to 2ft in thickness. This band shows current bedding.

Another bed is present in Lulung, which is 4km from Mawryngkneng police outpost towards Jowai. The thickness of this bed is about 100m and striking in the NE-SW direction with dip (40^0 to 78^0) towards NW. The conglomerate beds are composed mostly of quartz and quartzites pebbles. The pebbles are mostly flat and rarely spherical. The present study attempts to evaluate the strain history of the pebbles using the methods developed by Flinn1952, Hossack 1968 and Ramsay 1967. From the flat pebbles and axial plane of the folds, it is clear that the principal stress acted across the main strikes of the rocks, i.e. in the NW-SE direction.

4.5.2 Methodology

Suitable locations of different positions of each bed are taken for measuring the intercepts of the pebbles and at least 50 pebbles are measured for each location. Five locations are selected for measuring the intercepts of the pebbles (two from the Mawryngkneng conglomerate bed and three from Lulung conglomerate bed). The azimuth directions and angle of inclination of

the intercepts of the pebbles are measured with the help of clinometer compass.

For strain analysis, measurement of three intercepts of the pebbles, from one of the conglomerate bed, maximum X, intermediate Y and minimum Z are taken. The pebbles are so tightly packed that these cannot be removed by hand easily. So the study is limited to 50 pebbles only taken through random sampling. To separate the pebbles little tapping with hammer is necessary.

The three intercepts of the pebbles had been measured in the field with the help of slide calipers and scale in centimeter units. Before removing the pebbles from the beds, the azimuth directions and angle of inclination of the intercepts of the pebbles are measured with the help of Brunton compass and later in the laboratory are plotted on a Wulf's net to determine the orientation of the pebbles. Shape factor (κ), three dimensional finite strain and symmetry of strain ellipsoid are determined by the methods employed by (Flinn1962, 1965, Nadai 1963 and Hossack 1968).

4.5.3 Orientation of pebbles

The conglomerate beds with high angle of inclination are characterized by non-spherical pebbles. The longest, intermediate and shortest axes of the ellipsoidal pebbles are designated as X, Y and Z respectively so that $X \geq Y \geq Z$. The lengths of the pebbles along X, Y and Z axes have been measured.

Bar diagram is prepared to show the frequency of orientation of X axes with reference to dip direction of S_0 (Fig-4.26a). Peak of the bar diagram expresses a recognizable preferred distribution of long axes. The pebbles are elongated in S_0 with the shortest axes Z normal to S_0, intermediate axes Y in

S_0 with a NW-SE trend and longest axes X in S_0 with a NE-SW trend. The regional plunge of the pebble elongation direction X is gently towards the SW. Poles of the conglomerate bed from its measured attitudes at each random sampling site of the pebbles were plotted in stereographic net to get a π-diagram (Fig-4.26b). Direction and inclination of the long axes of the pebbles were plotted on a stereographic net to show X axis orientation (Fig-4.26d). A π-diagram is also prepared to show the Z axis orientation of the pebbles (Fig-4.26c).

From these figures, it may be stated that recognizable dimensional preferred orientation of X axis of the pebbles spread over the conglomerate bed S_0 almost oriented parallel to strike of the conglomerate bed. In some of the exposures the long axes are distinctly angular to S_0 plane indicating that the deformation was mild and it was not strong enough to bring XY plane of the pebbles parallel to S_0.

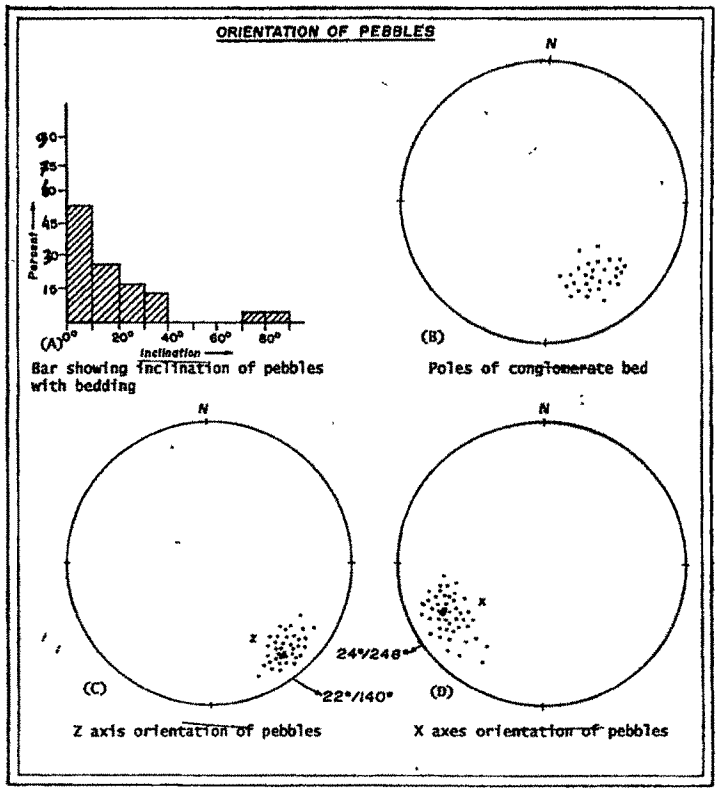

Fig-4.26: Oriantation of pebbles.

4.5.4 Strain analysis

Pebbles were used as various strain makers from the different areas (Burns and Spry 1969, Lisle 1979, Singh and Thakur 1989, Bhatt and Saklani 1990. Gairola and Hatwal 1991). In order to discuss the strain at a point two different kinds of quantities are required. One measures the relative changes of length of lines and the other measures the changes in the angles between pairs of lines.

The principal extension value of the pebbles viz. X,Y and Z are divided by 2 to obtain the principal finite strain of length$(1+e_1)$, $(1+e_2)$and $(1+e_3)$ along the long, intermediate and short axes respectively, where e represents engineering strain(Table-4.5, 4.6, 4.7, 4.8& 4.9). The shapes of the strain ellipsoids were determined by plotting the ratios $(1+e_1)/ (1+e_2)$ =a, as ordinate and $(1+e_2)/ (1+e_3)$ =b, as abscissa in Flinn's 1962 graph. The plots reveal that majority of them lie in the flattening field and a few plots lie in the constriction field (Fig-4.27a, b, c, d&e). The 'κ 'value for the arithmetic mean shape of the strain ellipsoid have been calculated from the mean value of $(1+e_1)$, $(1+e_2)$ and $(1+e_3)$ with the help of the following equations given by Flinn 1962.

$$K= [\{(1+e_1)/ (1+e_2)\}-1]/ [\{(1+e_2)/ (1+e_3)\}-1] \text{ ---------- (1)}$$

By putting the values of 'a' and 'b' in the equation-1, the value of 'κ' for the mean shape of the strain ellipsoid are calculated. The 'κ' values of the three station of Lulang conglomerate are 0.67, 0.87 and 0.80. The value of 'κ' for two station of Mawryngkneng conglomerate has been calculated out to be 0.70 and 0.80. The 'κ' values shows that the mean strain ellipsoid is of flattening type and lies close to the plane strain type ellipsoid for both the conglomerate beds.

TABLE : 4.5 Strain analysis data for Lulung conglomerate

									A	B	C	D	E	F	G	H	I	J
Sl no	X(in cm)	Y(in cm)	Z(in cm)	r^3=XYZ	r	log X/r	log Y/r	log Z/r	$(1+e_1)$	$(1+e_2)$	$(1+e_3)$	$(\log A/B)^2$	$(\log B/C)^2$	$(\log C/A)^2$	K= (logA/B)/ (log B/C)	V=(1-K)/ (1+K)	$2/3(D+E+F)^{1/2}$	$\bar{\varepsilon}_s = [(\sqrt{3})/2]I$
1	5.0	3.5	2.0	35.00	3.27	0.18	0.03	-0.21	2.50	1.75	1.00	0.02	0.06	0.16	0.64	0.22	0.33	0.28
2	3.8	3.5	1.2	15.96	2.52	0.18	0.14	-0.32	1.90	1.75	0.60	0.00	0.22	0.25	0.08	0.86	0.46	0.39
3	5.0	2.5	1.8	22.50	2.82	0.25	-0.05	-0.20	2.50	1.25	0.90	0.09	0.02	0.20	2.11	-0.36	0.37	0.32
4	4.0	2.7	1.0	10.80	2.21	0.26	0.09	-0.34	2.00	1.35	0.50	0.03	0.19	0.36	0.40	0.43	0.51	0.44
5	2.5	2.0	0.6	3.00	1.44	0.24	0.14	-0.38	1.25	1.00	0.30	0.01	0.27	0.38	0.19	0.69	0.54	0.47
6	5.0	3.0	1.5	22.50	2.82	0.25	0.03	-0.27	2.50	1.50	0.75	0.05	0.09	0.27	0.74	0.15	0.43	0.37
7	2.1	1.8	0.6	2.27	1.31	0.20	0.14	-0.34	1.05	0.90	0.30	0.00	0.23	0.30	0.14	0.75	0.48	0.42
8	3.5	2.0	0.8	5.60	1.78	0.29	0.05	-0.35	1.75	1.00	0.40	0.06	0.16	0.41	0.61	0.24	0.53	0.46
9	3.2	2.3	1.0	7.36	1.95	0.22	0.07	-0.29	1.60	1.15	0.50	0.02	0.13	0.26	0.40	0.43	0.42	0.37
10	3.5	1.8	1.2	7.56	1.96	0.25	-0.04	-0.21	1.75	0.90	0.60	0.08	0.03	0.22	1.64	-0.24	0.38	0.33
11	4.0	3.0	1.2	14.40	2.43	0.22	0.09	-0.31	2.00	1.50	0.60	0.02	0.16	0.27	0.31	0.52	0.45	0.39
12	5.0	4.0	2.0	40.00	3.42	0.16	0.07	-0.23	2.50	2.00	1.00	0.01	0.09	0.16	0.32	0.51	0.34	0.29
13	5.0	4.0	1.5	30.00	3.11	0.21	0.11	-0.32	2.50	2.00	0.75	0.01	0.18	0.27	0.23	0.63	0.45	0.39
14	4.7	3.2	1.5	22.56	2.83	0.22	0.05	-0.28	2.35	1.60	0.75	0.03	0.11	0.25	0.51	0.33	0.41	0.36
15	4.2	2.5	0.8	8.40	2.03	0.32	0.09	-0.41	2.10	1.25	0.40	0.05	0.24	0.52	0.46	0.37	0.60	0.52
16	4.5	2.3	1.0	10.35	2.18	0.31	0.02	-0.34	2.25	1.15	0.50	0.08	0.13	0.43	0.81	0.11	0.53	0.46
17	3.3	1.7	0.5	2.81	1.41	0.37	0.08	-0.45	1.65	0.85	0.25	0.08	0.28	0.67	0.54	0.30	0.68	0.59
18	2.5	1.7	0.8	3.40	1.50	0.22	0.05	-0.27	1.25	0.85	0.40	0.03	0.11	0.24	0.51	0.32	0.41	0.36
19	2.7	2.0	1.0	5.40	1.75	0.19	0.06	-0.24	1.35	1.00	0.50	0.02	0.09	0.19	0.43	0.40	0.36	0.31
20	2.2	2.0	1.0	4.40	1.64	0.13	0.09	-0.21	1.10	1.00	0.50	0.00	0.09	0.12	0.14	0.76	0.30	0.26
21	3.8	2.6	1.1	10.87	2.22	0.23	0.07	-0.30	1.90	1.30	0.55	0.03	0.14	0.29	0.44	0.39	0.45	0.39
22	4.5	2.3	1.2	12.42	2.32	0.29	0.00	-0.29	2.25	1.15	0.60	0.08	0.08	0.33	1.03	-0.02	0.47	0.41
23	2.6	1.7	0.6	2.65	1.38	0.27	0.09	-0.36	1.30	0.85	0.30	0.03	0.20	0.41	0.41	0.42	0.53	0.46
24	2.8	1.7	0.6	2.86	1.42	0.30	0.08	-0.37	1.40	0.85	0.30	0.05	0.20	0.45	0.48	0.35	0.56	0.48
25	2.5	1.8	0.5	2.25	1.31	0.28	0.14	-0.42	1.25	0.90	0.25	0.02	0.31	0.49	0.26	0.59	0.60	0.52

Contd

									A	B	C	D	E	F	G	H	I	J
Sl no	X(in cm)	Y(in cm)	Z(in cm)	r^3=XYZ	r	log X/r	log Y/r	log Z/r	$(1+e_1)$	$(1+e_2)$	$(1+e_3)$	$(logA/B)^2$	$(logB/C)^2$	$(logC/A)^2$	K= (logA/B)/ (log B/C)	V=(1-K)/ (1+K)	$2/3(D+E+F)^{1/2}$	$\bar{\varepsilon}_i = [(\sqrt{3})/2]I$
26	2 7	2.5	1.0	6.75	1.89	0.15	0.12	-0.28	1.35	1.25	0.50	0.00	0.16	0.19	0 08	0 85	0 39	0 34
27	2 0	1.4	0.5	1.40	1.12	0.25	0.10	-0.35	1.00	0.70	0.25	0.02	0.20	0 36	0.35	0 49	0.51	0.44
28	2.8	2.0	0.6	3 36	1.50	0.27	0.13	-0.40	1.40	1.00	0.30	0 02	0 27	0 45	0.28	0.56	0 57	0 50
29	2 6	1.7	0.7	3.09	1.46	0.25	0.07	-0.32	1.30	0.85	0 35	0.03	0.15	0 32	0 48	0 35	0 47	0.41
30	2 5	1.5	0.7	2.63	1 38	0.26	0.04	-0.29	1.25	0 75	0 35	0.05	0.11	0.31	0 67	0 20	0 45	0 39
31	3 5	2.0	0.5	3.50	1.52	0.36	0.12	-0.48	1.75	1.00	0.25	0 06	0 36	0 71	0.40	0.42	0 71	0 61
32	2.7	2.0	0.7	3.78	1.56	0.24	0.11	-0.35	1.35	1.00	0.35	0.02	0.21	0.34	0.29	0.56	0.50	0 43
33	2.5	2.0	0.6	3.00	1.44	0.24	0.14	-0.38	1.25	1.00	0.30	0.01	0.27	0.38	0.19	0.69	0.54	0.47
34	2.0	1.7	0.5	1.70	1.19	0.22	0.15	-0.38	1.00	0.85	0.25	0.00	0.28	0.36	0.13	0.77	0.54	0 46
35	2.2	1.2	0.5	1.32	1.10	0.30	0.04	-0.34	1.10	0.60	0.25	0.07	0.14	0 41	0.69	0.18	0.53	0 46
36	4.0	2.5	1.5	15.00	2.47	0.21	0.01	-0.22	2.00	1.25	0.75	0.04	0.05	0.18	0.92	0.04	0.35	0 30
37	4 3	1.8	1.0	7.74	1.98	0.34	-0.04	-0.30	2.15	0.90	0.50	0.14	0.07	0.40	1.48	-0.19	0.52	0 45
38	2.7	1.6	0.5	2.16	1.29	0.32	0.09	-0.41	1.35	0.80	0.25	0.05	0.26	0.54	0.45	0.38	0.61	0 53
39	3.0	1.5	0.9	4.05	1.59	0.27	-0.03	-0.25	1.50	0.75	0.45	0.09	0.05	0.27	1.36	-0.15	0.43	0.37
40	2 2	2.0	0.5	2.20	1.30	0.23	0.19	-0.42	1.10	1.00	0.25	0.00	0.36	0.41	0.07	0.87	0.59	0 51
41	1.5	1.2	0.3	0.54	0.81	0.27	0.17	-0.43	0.75	0.60	0.15	0.01	0.36	0.49	0.16	0.72	0.62	0 53
42	2.4	2.0	0.4	1.92	1.24	0.29	0.21	-0.49	1.20	1.00	0.20	0.01	0.49	0.61	0.11	0.80	0.70	0.61
43	3.0	2.5	0.6	4.50	1.65	0.26	0.18	-0.44	1.50	1.25	0.30	0.01	0.38	0.49	0.13	0.77	0.62	0 54
44	3 5	2.5	1.0	8.75	2.06	0.23	0.08	-0.31	1.75	1.25	0.50	0.02	0.16	0 30	0.37	0.46	0 46	0.40
45	4 5	4.0	1.5	27.00	3.00	0.18	0.12	-0.30	2.25	2.00	0.75	0.00	0.18	0.23	0.12	0.79	0 43	0 37
46	2 8	1.8	0.8	4.03	1.59	0.25	0.05	-0.30	1.40	0.90	0.40	0 04	0.12	0 30	0.54	0 29	0.45	0 39
47	2 0	1.4	0 5	1.40	1.12	0.25	0.10	-0.35	1.00	0.70	0.25	0.02	0.20	0.36	0.35	0.49	0 51	0.44
48	1.8	1.0	0 4	0.72	0.90	0.30	0.05	-0.35	0.90	0.50	0.20	0 07	0.16	0.43	0.64	0 22	0.54	0 47
49	2 2	1 5	1 0	3.30	1.49	0.17	0.00	-0.17	1.10	0.75	0.50	0.03	0.03	0 12	0.94	0.03	0 28	0 24
50	1.8	1 2	0 6	1 30	1.09	0.22	0 04	-0.26	0 90	0.60	0.30	0.03	0.09	0 23	0.58	0 26	0 39	0.34
Average	3.21	2.18	0.90	8.55	1.83	0.25	0.08	-0.33	1.61	1.09	0.45	0.04	0.18	0.34	0.51	0.40	0.49	0.42

TABLE : 4.6 Strain analysis data for Lulung conglomerate

									A	B	C	D	E	F	G	H	I	J
Sl no	X(in cm)	Y(in cm)	Z(in cm)	r^3=XYZ	r	log X/r	log Y/r	log Z/r	$(1+e_1)$	$(1+e_2)$	$(1+e_3)$	$(\log A/B)^2$	$(\log B/C)^2$	$(\log C/A)^2$	K= (logA/B)/ (log B/C)	V=(1-K)/ (1+K)	$2/3(D+E+F)^{1/2}$	$\bar{\varepsilon}_s$ = [(√3)/2]I
1	6.0	4.0	2.0	48.00	3.63	0.22	0.04	-0.26	3.00	2.00	1.00	0.03	0.09	0.23	0.58	0.26	0.39	0.34
2	5.4	2.7	1.0	14.58	2.44	0.34	0.04	-0.39	2.70	1.35	0.50	0.09	0.19	0.54	0.70	0.18	0.60	0.52
3	6.0	3.5	2.0	42.00	3.48	0.24	0.00	-0.24	3.00	1.75	1.00	0.05	0.06	0.23	0.96	0.02	0.39	0.34
4	6.0	2.5	0.6	9.00	2.08	0.46	0.08	-0.54	3.00	1.25	0.30	0.14	0.38	1.00	0.61	0.24	0.82	0.71
5	6.0	3.0	1.8	32.40	3.19	0.27	-0.03	-0.25	3.00	1.50	0.90	0.09	0.05	0.27	1.36	-0.15	0.43	0.37
6	4.0	2.0	0.5	4.00	1.59	0.40	0.10	-0.50	2.00	1.00	0.25	0.09	0.36	0.82	0.50	0.33	0.75	0.65
7	4.5	3.0	1.2	16.20	2.53	0.25	0.07	-0.32	2.25	1.50	0.60	0.03	0.16	0.33	0.44	0.39	0.48	0.42
8	4.5	2.5	1.0	11.25	2.24	0.30	0.05	-0.35	2.25	1.25	0.50	0.07	0.16	0.43	0.64	0.22	0.54	0.47
9	4.0	3.0	1.0	12.00	2.29	0.24	0.12	-0.36	2.00	1.50	0.50	0.02	0.23	0.36	0.26	0.58	0.52	0.45
10	6.5	2.5	0.5	8.13	2.01	0.51	0.09	-0.60	3.25	1.25	0.25	0.17	0.49	1.24	0.59	0.25	0.92	0.80
11	4.1	2.3	1.0	9.43	2.11	0.29	0.04	-0.32	2.05	1.15	0.50	0.06	0.13	0.38	0.69	0.18	0.50	0.44
12	6.0	2.8	1.0	16.80	2.56	0.37	0.04	-0.41	3.00	1.40	0.50	0.11	0.20	0.61	0.74	0.15	0.64	0.55
13	8.0	5.0	2.0	80.00	4.31	0.27	0.06	-0.33	4.00	2.50	1.00	0.04	0.16	0.36	0.51	0.32	0.50	0.43
14	4.8	2.6	1.4	17.47	2.59	0.27	0.00	-0.27	2.40	1.30	0.70	0.07	0.07	0.29	0.99	0.00	0.44	0.38
15	4.0	2.0	0.8	6.40	1.86	0.33	0.03	-0.37	2.00	1.00	0.40	0.09	0.16	0.49	0.76	0.14	0.57	0.50
16	4.2	1.3	0.5	2.73	1.40	0.48	-0.03	-0.45	2.10	0.65	0.25	0.26	0.17	0.85	1.23	-0.10	0.76	0.65
17	5.0	3.5	1.2	21.00	2.76	0.26	0.10	-0.36	2.50	1.75	0.60	0.02	0.22	0.38	0.33	0.50	0.53	0.46
18	5.5	4.0	2.8	61.60	3.95	0.14	0.01	-0.15	2.75	2.00	1.40	0.02	0.02	0.09	0.89	0.06	0.24	0.21
19	4.0	2.0	0.5	4.00	1.59	0.40	0.10	-0.50	2.00	1.00	0.25	0.09	0.36	0.82	0.50	0.33	0.75	0.65
20	6.0	4.0	1.7	40.80	3.44	0.24	0.07	-0.31	3.00	2.00	0.85	0.03	0.14	0.30	0.47	0.36	0.46	0.40
21	8.0	2.1	0.7	11.76	2.27	0.55	-0.03	-0.51	4.00	1.05	0.35	0.34	0.23	1.12	1.22	-0.10	0.86	0.75
22	6.0	1.5	0.4	3.60	1.53	0.59	-0.01	-0.58	3.00	0.75	0.20	0.36	0.33	1.38	1.05	-0.02	0.96	0.83
23	7.5	2.5	0.5	9.38	2.11	0.55	0.07	-0.63	3.75	1.25	0.25	0.23	0.49	1.38	0.68	0.19	0.96	0.84
24	5.0	2.3	0.9	10.35	2.18	0.36	0.02	-0.38	2.50	1.15	0.45	0.11	0.17	0.55	0.83	0.09	0.61	0.53
25	5.5	1.4	0.5	3.85	1.57	0.55	-0.05	-0.50	2.75	0.70	0.25	0.35	0.20	1.08	1.33	-0.14	0.85	0.74

Contd

									A	B	C	D	E	F	G	H	I	J
Sl no	X(in cm)	Y(in cm)	Z(in cm)	r^3=XYZ	r	log X/r	log Y/r	log Z/r	$(1+e_1)$	$(1+e_2)$	$(1+e_3)$	$(\log A/B)^2$	$(\log B/C)^2$	$(\log C/A)^2$	K= (logA/B)/ (log B/C)	V=(1-K)/ (1+K)	$2/3(D+E+F)^{1/2}$	$\bar{\varepsilon}_s = [(\sqrt{3})/2]I$
26	6.5	2.5	1.0	16.25	2.53	0.41	-0.01	-0.40	3.25	1.25	0.50	0.17	0.16	0.66	1.04	-0.02	0 66	0.57
27	4.0	1.5	1.0	6.00	1.82	0.34	-0.08	-0.26	2.00	0.75	0.50	0.18	0 03	0.36	2 42	-0 42	0.50	0 44
28	4.0	3.0	1 5	18.00	2 62	0.18	0.06	-0.24	2.00	1.50	0.75	0.02	0.09	0 18	0 42	0.41	0 36	0 31
29	6 0	2 8	1 6	26.88	3.00	0.30	-0.03	-0.27	3.00	1.40	0.80	0.11	0.06	0.33	1 36	-0.15	0 47	0.41
30	6 0	2.8	1 8	30.24	3.12	0.28	-0.05	-0.24	3.00	1.40	0.90	0.11	0.04	0.27	1 72	-0 27	0 43	0.37
31	5 5	2.9	1.5	23.93	2.88	0.28	0.00	-0.28	2.75	1.45	0.75	0.08	0.08	0 32	0.97	0.01	0 46	0 40
32	6 0	2.5	1.0	15.00	2.47	0.39	0.01	-0.39	3.00	1.25	0.50	0.14	0.16	0 61	0.96	0.02	0 63	0 55
33	7.5	3.0	0 8	18.00	2.62	0.46	0.06	-0.52	3.75	1.50	0.40	0.16	0 33	0.94	0.69	0 18	0 80	0.69
34	5.0	3 2	1.9	30.40	3.12	0.20	0.01	-0.22	2.50	1.60	0.95	0.04	0 05	0.18	0.86	0 08	0 34	0.30
35	4 4	1.6	1.0	7 04	1.92	0.36	-0.08	-0.28	2.20	0.80	0.50	0.19	0.04	0.41	2.15	-0 37	0.54	0 46
36	4 0	2 5	1.8	18.00	2.62	0.18	-0.02	-0.16	2.00	1.25	0.90	0.04	0.02	0.12	1.43	-0.18	0.28	0 25
37	6.5	3.9	2.0	50.70	3.70	0.24	0.02	-0.27	3.25	1.95	1.00	0.05	0.08	0.26	0.76	0 13	0.42	0.36
38	4.2	3 0	1.7	21.42	2.78	0.18	0.03	-0.21	2.10	1.50	0.85	0.02	0.06	0.15	0.59	0.26	0 32	0.28
39	8.0	1.8	0.5	7.20	1.93	0.62	-0.03	-0.59	4.00	0.90	0.25	0.42	0.31	1 45	1.16	-0.08	0.98	0.85
40	4.0	2.5	1.8	18.00	2.62	0.18	-0.02	-0.16	2.00	1.25	0.90	0.04	0.02	0.12	1.43	-0 18	0 28	0.25
41	6.0	2 8	1.5	25.20	2.93	0.31	-0.02	-0.29	3.00	1.40	0.75	0.11	0.07	0.36	1.22	-0.10	0 49	0 43
42	6.0	3.9	1.0	23.40	2.86	0.32	0.13	-0.46	3.00	1.95	0.50	0.04	0.35	0.61	0 32	0.52	0 66	0.57
43	2.4	1.6	1.0	3.84	1.57	0.19	0.01	-0.19	1.20	0.80	0.50	0.03	0.04	0.14	0.86	0.07	0.31	0 27
44	3.0	2.0	0.6	3.60	1.53	0.29	0.12	-0.41	1.50	1.00	0.30	0.03	0 27	0.49	0.34	0 50	0.59	0.51
45	4.1	3.2	2.1	27.55	3.02	0.13	0.03	-0.16	2.05	1.60	1.05	0.01	0 03	0.08	0.59	0 26	0.24	0.21
46	5.4	4 3	2.2	51.08	3.71	0.16	0 06	-0.23	2.70	2.15	1.10	0.01	0.08	0.15	0.34	0.49	0 33	0.29
47	4 9	3 7	1.5	27.20	3.01	0.21	0.09	-0.30	2.45	1.85	0.75	0.01	0.15	0.26	0.31	0.53	0 44	0 38
48	4 0	2.5	1.3	13 00	2.35	0.23	0.03	-0.26	2.00	1.25	0.65	0.04	0.08	0.24	0.72	0 16	0.40	0 35
49	3 6	2.7	2 0	19.44	2.69	0.13	0.00	-0.13	1.80	1.35	1.00	0 02	0.02	0 07	0 96	0 02	0 21	0 18
50	6 0	3.0	1.7	30.60	3.13	0.28	-0.02	-0 26	3.00	1.50	0.85	0.09	0.06	0.30	1.22	-0 10	0 45	0 39
Average	5.27	2.74	1.27	20.57	2.56	0.32	0.03	-0.34	2.64	1.37	0.63	0.10	0.16	0.49	0.87	0.12	0.54	0.47

TABLE : 4.7 Strain analysis data for Lulung conglomerate

									A	B	C	D	E	F	G	H	I	J
Sl no	X(in cm)	Y(in cm)	Z(In cm)	r^3=XYZ	r	log X/r	log Y/r	log Z/r	$(1+e_1)$	$(1+e_2)$	$(1+e_3)$	$(\log A/B)^2$	$(\log B/C)^2$	$(\log C/A)^2$	K= (logA/B)/ (log B/C)	V=(1-K)/ (1+K)	$2/3(D+E+F)^{1/2}$	$\bar{\varepsilon}_s$ = [(√3)/2]I
1	4.0	2.0	1.5	12.00	2.29	0.24	-0.06	-0.18	2.00	1.00	0.75	0.09	0.02	0.18	2.41	-0.41	0.36	0.31
2	3.0	2.0	1.2	7.20	1.93	0.19	0.02	-0.21	1.50	1.00	0.60	0.03	0.05	0.16	0.79	0 11	0.33	0 28
3	2.5	2.0	1.0	5.00	1.71	0.16	0.07	-0.23	1.25	1.00	0.50	0 01	0 09	0.16	0.32	0 51	0 34	0 29
4	3.9	3.2	2.0	24.96	2.92	0.13	0.04	-0.16	1.95	1.60	1.00	0.01	0.04	0.08	0 42	0.41	0 24	0.21
5	4.5	3.0	2.1	28.35	3.05	0.17	-0.01	-0.16	2.25	1.50	1.05	0.03	0.02	0 11	1 14	-0.06	0.27	0.23
6	3.0	2.5	1.5	11.25	2.24	0.13	0.05	-0.17	1.50	1.25	0.75	0.01	0.05	0.09	0 36	0.47	0 25	0 22
7	4.0	3.5	0.5	7.00	1.91	0.32	0.26	-0.58	2.00	1.75	0.25	0.00	0.71	0.82	0.07	0.87	0.82	0 71
8	3.5	2.9	0.8	8.12	2.01	0.24	0.16	-0.40	1.75	1.45	0.40	0.01	0.31	0 41	0 15	0 75	0 57	0 49
9	1.5	1.2	0.5	0.90	0 97	0.19	0.09	-0.29	0 75	0.60	0.25	0.01	0 14	0.23	0.25	0 59	0.41	0.36
10	7.0	5.7	1.5	59.85	3.91	0.25	0.16	-0.42	3.50	2.85	0.75	0.01	0.34	0.45	0 15	0 73	0.59	0 51
11	6.5	5.7	1.4	51.87	3.73	0.24	0.18	-0.43	3.25	2.85	0.70	0.00	0 37	0.44	0.09	0.83	0.60	0.52
12	9.0	4.5	2.0	81.00	4.33	0.32	0.02	-0.34	4.50	2.25	1.00	0.09	0.12	0.43	0.85	0 08	0 53	0 46
13	5.0	3.0	1.1	16 50	2.55	0.29	0.07	-0.36	2.50	1.50	0.55	0.05	0.19	0.43	0 51	0.33	0.55	0 47
14	7.0	3 1	2.0	43.40	3.51	0.30	-0.05	-0.24	3.50	1.55	1.00	0.13	0.04	0.30	1.86	-0 30	0.45	0 39
15	5.5	4 0	2.0	44.00	3.53	0.19	0.05	-0.25	2.75	2.00	1.00	0.02	0.09	0.19	0 46	0.37	0 37	0 32
16	5.0	3.5	2.0	35.00	3.27	0.18	0.03	-0.21	2.50	1.75	1.00	0.02	0 06	0.16	0.64	0 22	0 33	0 28
17	3.5	3.0	1.5	15.75	2.51	0.14	0.08	-0.22	1.75	1.50	0.75	0.00	0 09	0.14	0.22	0.64	0.32	0 28
18	7 0	4.5	2.0	63.00	3.98	0.25	0.05	-0.30	3.50	2.25	1.00	0.04	0.12	0 30	0.54	0.29	0 45	0.39
19	5 0	3.5	2.3	40.25	3.43	0.16	0.01	-0.17	2.50	1.75	1.15	0.02	0.03	0.11	0.85	0.08	0 28	0.24
20	7.0	5.0	2.5	87.50	4 44	0.20	0.05	-0.25	3.50	2.50	1.25	0.02	0 09	0.20	0.49	0.35	0 37	0 32
21	5.0	2.5	1.5	18.75	2.66	0.27	-0 03	-0.25	2.50	1.25	0.75	0.09	0.05	0.27	1.36	-0.15	0 43	0 37
22	3.5	2.5	1.0	8.75	2.06	0.23	0.08	-0.31	1.75	1.25	0.50	0.02	0.16	0.30	0.37	0.46	0.46	0 40
23	6 0	4 5	2.0	54.00	3.78	0.20	0.08	-0.28	3.00	2.25	1.00	0.02	0.12	0.23	0.35	0.48	0.40	0.35
24	5.0	4 5	2.1	47.25	3.62	0.14	0.10	-0.24	2.50	2.25	1.05	0.00	0.11	0.14	0 14	0.76	0.34	0.29
25	7.0	3 5	2.0	49 00	3.66	0.28	-0.02	-0.26	3.50	1.75	1.00	0.09	0.06	0.30	1.24	-0.11	0.44	0 39

Contd

									A	B	C	D	E	F	G	H	I	J
Sl no	X(In cm)	Y(in cm)	Z(In cm)	r^3=XYZ	r	log X/r	log Y/r	log Z/r	$(1+e_1)$	$(1+e_2)$	$(1+e_3)$	$(logA/B)^2$	$(logB/C)^2$	$(logC/A)^2$	K= (logA/B)/ (log B/C)	V=(1-K)/ (1+K)	$2/3(D+E+F)^{1/2}$	$\bar{\varepsilon}_s = [(\sqrt{3})/2]I$
26	5.0	4.0	2.2	44.00	3.53	0.15	0.05	-0.21	2.50	2.00	1.10	0.01	0.07	0.13	0.37	0.46	0.30	0.26
27	4.5	2.5	1.0	11.25	2.24	0.30	0.05	-0.35	2.25	1.25	0.50	0.07	0.16	0.43	0.64	0.22	0.54	0.47
28	5 0	3.0	1.5	22.50	2.82	0.25	0.03	-0.27	2.50	1.50	0.75	0.05	0.09	0.27	0.74	0.15	0.43	0 37
29	6.0	2.0	1.0	12.00	2.29	0.42	-0.06	-0.36	3.00	1.00	0.50	0.23	0.09	0.61	1.58	-0.23	0.64	0.55
30	6.7	3.1	1.5	31.16	3.15	0.33	-0.01	-0.32	3.35	1.55	0.75	0.11	0.10	0.42	1.06	-0.03	0.53	0 46
31	5.0	3.0	1.0	15.00	2.47	0.31	0.09	-0.39	2.50	1.50	0.50	0.05	0.23	0.49	0.46	0.37	0.58	0 50
32	6.0	3 6	2.0	43.20	3.51	0.23	0.01	-0.24	3.00	1.80	1.00	0.05	0.07	0.23	0.87	0.07	0 39	0.34
33	8 5	3.7	1.6	50.32	3.69	0.36	0.00	-0.36	4.25	1.85	0.80	0.13	0.13	0 53	0 99	0 00	0 59	0.51
34	3.5	2 5	1.0	8 75	2.06	0.23	0.08	-0.31	1.75	1.25	0.50	0.02	0.16	0 30	0.37	0.46	0.46	0 40
35	3 5	2 0	1.0	7.00	1.91	0.26	0.02	-0.28	1.75	1.00	0.50	0.06	0.09	0.30	0.81	0 11	0.44	0 39
36	2 0	1.4	1.0	2.80	1.41	0.15	0.00	-0.15	1.00	0.70	0.50	0.02	0.02	0.09	1.06	-0 03	0.25	0 21
37	2.7	2.0	1.0	5.40	1.75	0.19	0.06	-0.24	1.35	1.00	0.50	0.02	0.09	0.19	0.43	0.40	0 36	0 31
38	2 5	1.1	1.0	2.75	1.40	0.25	-0.11	-0.15	1.25	0.55	0.50	0.13	0.00	0.16	8.61	-0.79	0.36	0.31
39	2.0	1.5	1.0	3.00	1.44	0.14	0.02	-0.16	1.00	0.75	0.50	0.02	0.03	0.09	0.71	0.17	0 25	0.21
40	3.0	2 0	1.0	6.00	1.82	0.22	0.04	-0.26	1.50	1.00	0.50	0.03	0.09	0.23	0.58	0.26	0.39	0 34
41	2.0	1.5	1.0	3.00	1.44	0.14	0.02	-0.16	1.00	0.75	0.50	0.02	0.03	0.09	0.71	0.17	0.25	0.21
42	2.5	2.0	1.5	7.50	1.96	0.11	0.01	-0.12	1.25	1.00	0.75	0.01	0.02	0.05	0.78	0.13	0.18	0.16
43	0.5	0.4	0.3	0.06	0.39	0.11	0.01	-0.12	0.25	0.20	0.15	0.01	0.02	0.05	0.78	0.13	0.18	0.16
44	2.0	1.4	0.5	1.40	1.12	0.25	0.10	-0.35	1.00	0.70	0.25	0.02	0.20	0.36	0.35	0.49	0.51	0.44
45	0.6	0.5	0.4	0.12	0.49	0.09	0.01	-0.09	0.30	0.25	0.20	0.01	0.01	0.03	0 82	0.10	0.14	0.12
46	2.0	1.5	0.7	2.10	1.28	0.19	0.07	-0.26	1.00	0.75	0.35	0.02	0.11	0.21	0.38	0.45	0.38	0.33
47	2 0	1.3	0.5	1.30	1.09	0.26	0.08	-0.34	1.00	0.65	0.25	0.04	0.17	0.36	0.45	0.38	0.50	0 44
48	2 3	1.5	1.0	3.45	1.51	0.18	0.00	-0.18	1.15	0.75	0.50	0.03	0.03	0.13	1 05	-0.03	0 30	0 26
49	2 5	1.5	0.6	2.25	1.31	0 28	0.06	-0.34	1.25	0.75	0.30	0.05	0.16	0.38	0.56	0.28	0.51	0.44
50	2 0	1 6	0.7	2.24	1.31	0.18	0.09	-0.27	1.00	0.80	0.35	0.01	0.13	0.21	0.27	0.57	0 39	0 34
Average	4.2	2.7	1.3	22.2	2.4	0.2	0.0	-0.3	2.1	1.4	0.7	0.0	0.1	0.3	0.8	0.3	0.4	0.4

TABLE :4.8 Strain analysis data for Mawryngkneng conglomerate

									A	B	C	D	E	F	G	H	I	J
Sl no	X(in cm)	Y(in cm)	Z(in cm)	r^3=XYZ	r	log X/r	log Y/r	log Z/r	$(1+e_1)$	$(1+e_2)$	$(1+e_3)$	$(\log A/B)^2$	$(\log B/C)^2$	$(\log C/A)^2$	K= (logA/B)/ (log B/C)	V=(1-K)/ (1+K)	$2/3(D+E+F)^{1/2}$	$\bar{\varepsilon}_s = [(\sqrt{3})/2]I$
1	1.5	1.0	0.5	0.75	0.91	0.22	0.04	-0.26	0.75	0.50	0.25	0.03	0.09	0.23	0.58	0.26	0 39	0.34
2	2.0	1.1	0.6	1.32	1 10	0.26	0.00	-0.26	1.00	0.55	0.30	0.07	0.07	0.27	0.99	0.01	0.43	0.37
3	1.4	1.2	0.6	1.01	1.00	0.14	0.08	-0.22	0.70	0.60	0.30	0.00	0.09	0.14	0.22	0.64	0.32	0.28
4	1 2	0.8	0.4	0.38	0.73	0.22	0.04	-0.26	0.60	0.40	0.20	0.03	0.09	0.23	0.58	0.26	0 39	0.34
5	1.7	1.5	0.7	1.79	1.21	0.15	0.09	-0.24	0.85	0.75	0.35	0.00	0.11	0.15	0.16	0.72	0 34	0.29
6	2.8	1.3	0.7	2.55	1.37	0.31	-0.02	-0.29	1.40	0.65	0.35	0.11	0.07	0.36	1.24	-0.11	0.49	0.43
7	1.3	0.9	0.4	0.47	0.78	0.22	0.06	-0.29	0.65	0.45	0.20	0.03	0.12	0.26	0.45	0.38	0.43	0.37
8	1.5	0.8	0.4	0 48	0.78	0.28	0.01	-0.29	0.75	0.40	0.20	0.07	0.09	0.33	0.91	0.05	0 47	0.41
9	1.8	1 0	0.5	0.90	0.97	0.27	0.02	-0.29	0 90	0.50	0.25	0.07	0.09	0.31	0.85	0.08	0 45	0.39
10	1 2	0.8	0.5	0.48	0.78	0.19	0.01	-0.19	0.60	0.40	0.25	0.03	0.04	0.14	0.86	0.07	0.31	0 27
11	2 5	1 8	0.7	3 15	1.47	0.23	0.09	-0.32	1.25	0.90	0.35	0.02	0.17	0.31	0.35	0.48	0.47	0.41
12	1.6	1 1	0.6	1.06	1.02	0.20	0.03	-0.23	0.80	0.55	0.30	0.03	0.07	0.18	0.62	0.24	0.35	0.30
13	1 7	1 3	0.4	0.88	0 96	0.25	0.13	-0.38	0.85	0.65	0.20	0.01	0.28	0.39	0.23	0.63	0.55	0 47
14	3.0	1 6	0.8	3.84	1 57	0.28	0.01	-0.29	1.50	0.80	0.40	0.07	0.09	0.33	0.91	0.05	0.47	0.41
15	1.4	1 0	0.3	0.42	0.75	0 27	0.13	-0.40	0.70	0.50	0.15	0.02	0.27	0.45	0.28	0.56	0.57	0.50
16	1 3	0 7	0.4	0.36	0 71	0.26	-0.01	-0.25	0.65	0.35	0.20	0.07	0.06	0.26	1.11	-0.05	0.42	0.36
17	1.2	0 8	0 3	0.29	0 66	0.26	0.08	-0.34	0.60	0 40	0.15	0.03	0.18	0.36	0.41	0.42	0 50	0.44
18	2.3	1 1	0 8	2.02	1 26	0 26	-0.06	-0.20	1.15	0.55	0.40	0.10	0.02	0.21	2.32	-0.40	0.38	0.33
19	1.4	0 8	0 3	0 34	0 70	0.30	0.06	-0.36	0 70	0 40	0.15	0.06	0.18	0.45	0.57	0 27	0.55	0 48
20	1 3	0 7	0.4	0 36	0 71	0.26	-0 01	-0.25	0 65	0 35	0 20	0 07	0.06	0.26	1.11	-0.05	0 42	0 36
21	1 3	0 7	0.4	0 36	0 71	0 26	-0.01	-0 25	0 65	0.35	0.20	0.07	0.06	0 26	1 11	-0.05	0.42	0.36
22	1 6	1 1	0 7	1 23	1 07	0.17	0.01	-0.19	0.80	0 55	0.35	0.03	0.04	0 13	0 83	0.09	0 29	0.25
23	1.4	1 0	0 4	0 56	0 82	0 23	0.08	-0 31	0 70	0.50	0.20	0.02	0.16	0.30	0 37	0 46	0 46	0 40
24	1 8	0 8	0.5	0.72	0 90	0.30	-0.05	-0.25	0 90	0 40	0 25	0.12	0.04	0.31	1.73	-0.27	0 46	0 40
25	1 6	1 0	0 4	0 64	0 86	0.27	0.06	-0.33	0.80	0 50	0 20	0.04	0.16	0.36	0 51	0.32	0 50	0.43

Contd

									A	B	C	D	E	F	G	H	I	J
Sl no	X(in cm)	Y(in cm)	Z(in cm)	r^3=XYZ	r	log X/r	log Y/r	log Z/r	$(1+e_1)$	$(1+e_2)$	$(1+e_3)$	$(logA/B)^2$	$(logB/C)^2$	$(logC/A)^2$	K= (logA/B)/ (log B/C)	V=(1-K)/ (1+K)	$2/3(D+E+F)^{1/2}$	$\bar{\varepsilon}_i = [(\sqrt{3})/2]I$
26	1.5	1.1	0.7	1.16	1.05	0.16	0.02	-0.18	0.75	0.55	0.35	0.02	0.04	0.11	0.69	0.19	0.27	0 24
27	2 0	1.8	0.6	2.16	1.29	0 19	0.14	-0.33	1.00	0.90	0.30	0.00	0 23	0.27	0.10	0.82	0.47	0 41
28	1.3	0.8	0.4	0.42	0.75	0.24	0.03	-0.27	0.65	0.40	0 20	0.04	0 09	0.26	0.70	0.18	0 42	0 36
29	3.0	1.6	1.0	4.80	1.69	0.25	-0.02	-0.23	1.50	0.80	0.50	0.07	0.04	0.23	1 34	-0.14	0 39	0 34
30	1.8	0.7	0.3	0.38	0.72	0.40	-0.01	-0.38	0.90	0.35	0.15	0.17	0.14	0.61	1.11	-0.05	0.64	0.55
31	2.8	2.0	0.9	5.04	1.71	0.21	0.07	-0.28	1.40	1.00	0.45	0.02	0.12	0 24	0 42	0.41	0.41	0 36
32	1.0	0.6	0.3	0.18	0.56	0.25	0.03	-0.27	0.50	0.30	0.15	0.05	0.09	0 27	0.74	0.15	0.43	0 37
33	3.1	2.2	1.1	7.50	1.96	0.20	0.05	-0.25	1.55	1.10	0.55	0.02	0.09	0.20	0.49	0.34	0 37	0.32
34	2.0	1.2	0.7	1.68	1.19	0.23	0.00	-0.23	1.00	0.60	0.35	0.05	0.05	0.21	0 95	0.03	0.37	0 32
35	2.0	1.5	0.6	1.80	1.22	0.22	0.09	-0.31	1.00	0.75	0.30	0.02	0.16	0.27	0.31	0.52	0.45	0.39
36	1.2	0.8	0.5	0.48	0.78	0.19	0.01	-0.19	0.60	0.40	0.25	0.03	0.04	0.14	0 86	0.07	0.31	0 27
37	1.2	0.9	0.3	0.32	0.69	0.24	0.12	-0.36	0.60	0.45	0.15	0.02	0.23	0.36	0.26	0.58	0.52	0 45
38	1.2	0.7	0.4	0.34	0.70	0.24	0.00	-0.24	0.60	0.35	0.20	0.05	0.06	0.23	0.96	0.02	0 39	0.34
39	1.4	1.0	0.3	0.42	0.75	0.27	0.13	-0.40	0.70	0.50	0.15	0.02	0 27	0.45	0.28	0.56	0.57	0 50
40	1.7	1.5	0.8	2.04	1.27	0.13	0.07	-0.20	0.85	0.75	0.40	0.00	0 07	0.11	0 20	0.67	0 29	0.25
41	1.5	0.8	0.4	0 48	0.78	0.28	0.01	-0.29	0.75	0.40	0.20	0.07	0.09	0.33	0 91	0.05	0 47	0 41
42	1.6	1.0	0.6	0.96	0.99	0.21	0.01	-0.22	0.80	0.50	0.30	0.04	0.05	0.18	0 92	0.04	0 35	0 30
43	1 6	1.2	0.4	0.77	0.92	0.24	0.12	-0.36	0 80	0.60	0.20	0.02	0.23	0.36	0 26	0.58	0 52	0 45
44	1.8	1.6	0.8	2.30	1.32	0.13	0.08	-0.22	0 90	0.80	0.40	0 00	0.09	0.12	0 17	0.71	0 31	0.27
45	2 0	1 6	0 7	2.24	1.31	0.18	0.09	-0.27	1 00	0.80	0.35	0.01	0 13	0.21	0 27	0 57	0 39	0 34
46	1.5	0.8	0.5	0.60	0.84	0.25	-0.02	-0.23	0.75	0.40	0.25	0.07	0.04	0 23	1 34	-0.14	0 39	0 34
47	1.7	1.3	0.6	1 33	1.10	0.19	0.07	-0.26	0 85	0 65	0.30	0 01	0.11	0.20	0 35	0.48	0.38	0 33
48	0.8	0 5	0.2	0 08	0.43	0.27	0.06	-0.33	0.40	0 25	0.10	0 04	0.16	0 36	0.51	0.32	0 50	0 43
49	2.4	1.7	0.7	2.86	1.42	0.23	0.08	-0.31	1 20	0 85	0.35	0.02	0.15	0.29	0 39	0.44	0.45	0 39
50	2.0	1 6	0.9	2.88	1.42	0.15	0.05	-0.20	1.00	0.80	0 45	0.01	0.06	0 12	0 39	0 44	0 29	0 25
Average	**1.7**	**1.1**	**0.6**	**1.4**	**1.0**	**0.2**	**0.0**	**-0.3**	**0.9**	**0.6**	**0.3**	**0.0**	**0.1**	**0.3**	**0.7**	**0.3**	**0.4**	**0.4**

TABLE :4.9 Strain analysis data for Mawryngkneng conglomerate

									A	B	C	D	E	F	G	H	I	J
Sl no	X(in cm)	Y(in cm)	Z(in cm)	r^3=XYZ	r	log X/r	log Y/r	log Z/r	$(1+e_1)$	$(1+e_2)$	$(1+e_3)$	$(logA/B)^2$	$(logB/C)^2$	$(logC/A)^2$	K= (logA/B)/ (log B/C)	V=(1-K)/ (1+K)	$2/3(D+E+F)^{1/2}$	$\bar{\varepsilon}_s = [(\sqrt{3})/2]I$
1	2.8	1.3	0.7	2.55	1.37	0.31	-0.02	-0.29	1.40	0.65	0.35	0.11	0.07	0.36	1 24	-0.11	0.49	0.43
2	2.7	1.6	0.5	2.16	1.29	0.32	0.09	-0.41	1.35	0.80	0.25	0.05	0.26	0.54	0.45	0.38	0.61	0.53
3	2.2	1.5	0,5	1.65	1.18	0.27	0.10	-0.37	1.10	0.75	0.25	0.03	0.23	0.41	0.35	0.48	0.54	0.47
4	2.0	1 2	0 3	0.72	0.90	0.35	0.13	-0.48	1.00	0.60	0.15	0.05	0.36	0.68	0.37	0.46	0.70	0 60
5	2.0	1.3	0.4	1.04	1.01	0.30	0.11	-0.40	1.00	0.65	0.20	0.04	0.26	0.49	0.37	0.46	0.59	0.51
6	3.4	2.4	1.3	10.61	2.20	0.19	0.04	-0.23	1.70	1.20	0.65	0.02	0.07	0.17	0.57	0.28	0.34	0.30
7	2.0	1.6	0.5	1.60	1.17	0.23	0.14	-0.37	1.00	0.80	0.25	0.01	0.26	0.36	0 19	0 68	0.53	0.46
8	1 7	1 4	0.4	0.95	0.98	0.24	0.15	-0.39	0.85	0.70	0.20	0.01	0.30	0.39	0 15	0.73	0.56	0.48
9	2 0	1 3	0.6	1.56	1.16	0.24	0.05	-0.29	1.00	0.65	0.30	0.04	0.11	0.27	0.56	0.28	0.43	0.37
10	2.7	1.4	0.5	1.89	1.24	0.34	0.05	-0.39	1.35	0.70	0.25	0.08	0.20	0.54	0.64	0.22	0 60	0 52
11	3.0	2.0	0.6	3.60	1.53	0.29	0.12	-0.41	1.50	1.00	0.30	0.03	0 27	0.49	0.34	0.50	0 59	0.51
12	1.9	1 3	0.5	1.24	1.07	0.25	0.08	-0.33	0.95	0.65	0.25	0.03	0 17	0.34	0.40	0.43	0.49	0 42
13	2.9	2 0	0.7	4.06	1.60	0.26	0.10	-0.36	1.45	1.00	0.35	0.03	0 21	0.38	0.35	0 48	0 52	0 45
14	2.7	1 6	0.6	2.59	1 37	0.29	0.07	-0.36	1.35	0.80	0.30	0 05	0.18	0.43	0 53	0 30	0.54	0.47
15	2.0	1 3	0.6	1.56	1.16	0.24	0.05	-0.29	1 00	0 65	0.30	0.04	0.11	0.27	0.56	0.28	0.43	0.37
16	2.1	1.9	0.5	2.00	1.26	0.22	0 18	-0.40	1.05	0.95	0 25	0.00	0.34	0.39	0 07	0 86	0.57	0 49
17	1.4	1 1	0.4	0.62	0 85	0 22	0.11	-0.33	0.70	0 55	0.20	0.01	0.19	0 30	0.24	0.61	0.47	0 41
18	1.2	0 8	0.4	0.38	0.73	0.22	0.04	-0.26	0 60	0 40	0.20	0.03	0 09	0.23	0.58	0 26	0 39	0.34
19	2.0	1.1	0.6	1.32	1.10	0.26	0 00	-0.26	1.00	0.55	0 30	0 07	0.07	0.27	0 99	0 01	0.43	0 37
20	1 7	1.2	0.6	1.22	1.07	0.20	0.05	-0.25	0.85	0.60	0.30	0.02	0 09	0.20	0 50	0.33	0 38	0 33
21	1.8	0.9	0.5	0.81	0.93	0 29	-0.02	-0.27	0.90	0 45	0.25	0 09	0.07	0.31	1.18	-0 08	0 45	0.39
22	1.2	0 7	0.4	0 34	0.70	0.24	0.00	-0.24	0.60	0.35	0.20	0.05	0.06	0.23	0 96.	0.02	0 39	0 34
23	2 0	1.2	0.5	1 20	1.06	0.27	0.05	-0.33	1.00	0.60	0.25	0 05	0.14	0 36	0 58	0 26	0 50	0 43
24	1 7	1.3	0.6	1.33	1.10	0.19	0.07	-0.26	0.85	0.65	0.30	0 01	0.11	0.20	0 35	0 48	0 38	0 33
25	1.3	1 1	0 4	0 57	0 83	0.19	0 12	-0.32	0.65	0 55	0.20	0.01	0.19	0.26	0 17	0 72	0 45	0 39

Contd

									A	B	C	D	E	F	G	H	I	J
Si no	X(In cm)	Y(In cm)	Z(In cm)	r^3=XYZ	r	log X/r	log Y/r	log Z/r	$(1+e_1)$	$(1+e_2)$	$(1+e_3)$	$(\log A/B)^2$	$(\log B/C)^2$	$(\log C/A)^2$	K= (logA/B)/ (log B/C)	V=(1-K)/ (1+K)	$2/3(D+E+F)^{1/2}$	$\bar{\varepsilon}_s = [(\sqrt{3})/2]I$
26	1.8	1.3	0.5	1.17	1.05	0.23	0.09	-0.32	0.90	0.65	0.25	0.02	0.17	0.31	0.34	0.49	0.47	0.41
27	1.8	1.2	0.6	1.30	1.09	0.22	0.04	-0.26	0.90	0.60	0.30	0.03	0.09	0.23	0.58	0.26	0.39	0.34
28	2.0	1.0	0.6	1.20	1.06	0.27	-0.03	-0.25	1.00	0.50	0.30	0.09	0.05	0.27	1.36	-0.15	0.43	0.37
29	1.8	1.2	0.7	1.51	1.15	0.20	0.02	-0.21	0.90	0.60	0.35	0.03	0.05	0.17	0.75	0.14	0.34	0 29
30	1 8	1.5	0.5	1.35	1.11	0.21	0.13	-0.34	0.90	0.75	0.25	0.01	0.23	0.31	0.17	0.72	0.49	0 43
31	3.0	2.0	1.0	6.00	1.82	0.22	0.04	-0.26	1.50	1.00	0.50	0.03	0.09	0 23	0.58	0 26	0.39	0 34
32	2.3	1.5	0.6	2 07	1.27	0.26	0.07	-0.33	1.15	0.75	0.30	0.03	0.16	0 34	0.47	0.36	0.49	0 42
33	1.5	1.0	0.4	0.60	0.84	0.25	0.07	-0.32	0.75	0.50	0.20	0.03	0.16	0 33	0 44	0.39	0.48	0.42
34	1 2	0 7	0 3	0.25	0.63	0.28	0.04	-0.32	0.60	0.35	0.15	0 05	0.14	0 36	0 64	0 22	0 50	0 43
35	1.5	1.0	0 3	0.45	0.77	0.29	0.12	-0.41	0.75	0.50	0.15	0 03	0 27	0.49	0 34	0 50	0.59	0 51
36	1 5	0.8	0 4	0.48	0.78	0.28	0.01	-0.29	0.75	0.40	0.20	0.07	0.09	0 33	0 91	0.05	0 47	0 41
37	2.0	1.2	0.5	1.20	1.06	0.27	0.05	-0.33	1.00	0.60	0.25	0.05	0.14	0.36	0.58	0 26	0 50	0.43
38	3 5	2.0	1.0	7 00	1.91	0.26	0.02	-0.28	1.75	1.00	0.50	0.06	0.09	0 30	0 81	0.11	0.44	0 39
39	2 5	1.1	1 0	2.75	1.40	0.25	-0.11	-0.15	1.25	0.55	0.50	0.13	0 00	0.16	8 61	-0.79	0 36	0 31
40	1 6	1.1	0.6	1.06	1.02	0.20	0.03	-0.23	0.80	0.55	0.30	0.03	0.07	0.18	0.62	0.24	0 35	0 30
41	3.0	1.6	0.8	3.84	1.57	0.28	0.01	-0.29	1.50	0.80	0.40	0.07	0.09	0.33	0.91	0 05	0.47	0.41
42	1 3	1.7	0.4	0.88	0.96	0.13	0.25	-0.38	0.65	0.85	0.20	0.01	0.39	0.26	-0 19	1.46	0.55	0.47
43	2 3	1.1	0.8	2.02	1.26	0.26	-0.06	-0.20	1.15	0.55	0.40	0.10	0.02	0.21	2 32	-0 40	0.38	0.33
44	1 6	1.1	0.7	1.23	1.07	0.17	0.01	-0.19	0.80	0.55	0.35	0 03	0.04	0.13	0 83	0.09	0 29	0 25
45	2.0	1 1	0.6	1 32	1.10	0.26	0.00	-0.26	1.00	0.55	0.30	0.07	0.07	0.27	0.99	0 01	0 43	0 37
46	2 4	1.4	0.9	3 02	1.45	0.22	-0.01	-0.21	1.20	0.70	0.45	0.05	0.04	0.18	1.22	-0 10	0 35	0 30
47	1.7	1 5	0.8	2.04	1.27	0.13	0.07	-0.20	0.85	0.75	0.40	0 00	0 07	0.11	0 20	0 67	0 29	0 25
48	1 6	1 0	0.6	0 96	0.99	0.21	0.01	-0.22	0 80	0.50	0.30	0.04	0 05	0 18	0 92	0 04	0 35	0 30
49	1.8	1.6	0.8	2 30	1 32	0.13	0.08	-0.22	0.90	0.80	0.40	0.00	0.09	0.12	0 17	0.71	0 31	0 27
50	1 5	0.8	0 5	0.60	0.84	0 25	-0.02	-0.23	0.75	0.40	0.25	0 07	0.04	0.23	1 34	-0 14	0 39	0 34
Average	**2.0**	**1.3**	**0.6**	**1.9**	**1.2**	**0.2**	**0.1**	**-0.3**	**1.0**	**0.7**	**0.3**	**0.0**	**0.1**	**0.3**	**0.8**	**0.3**	**0.5**	**0.4**

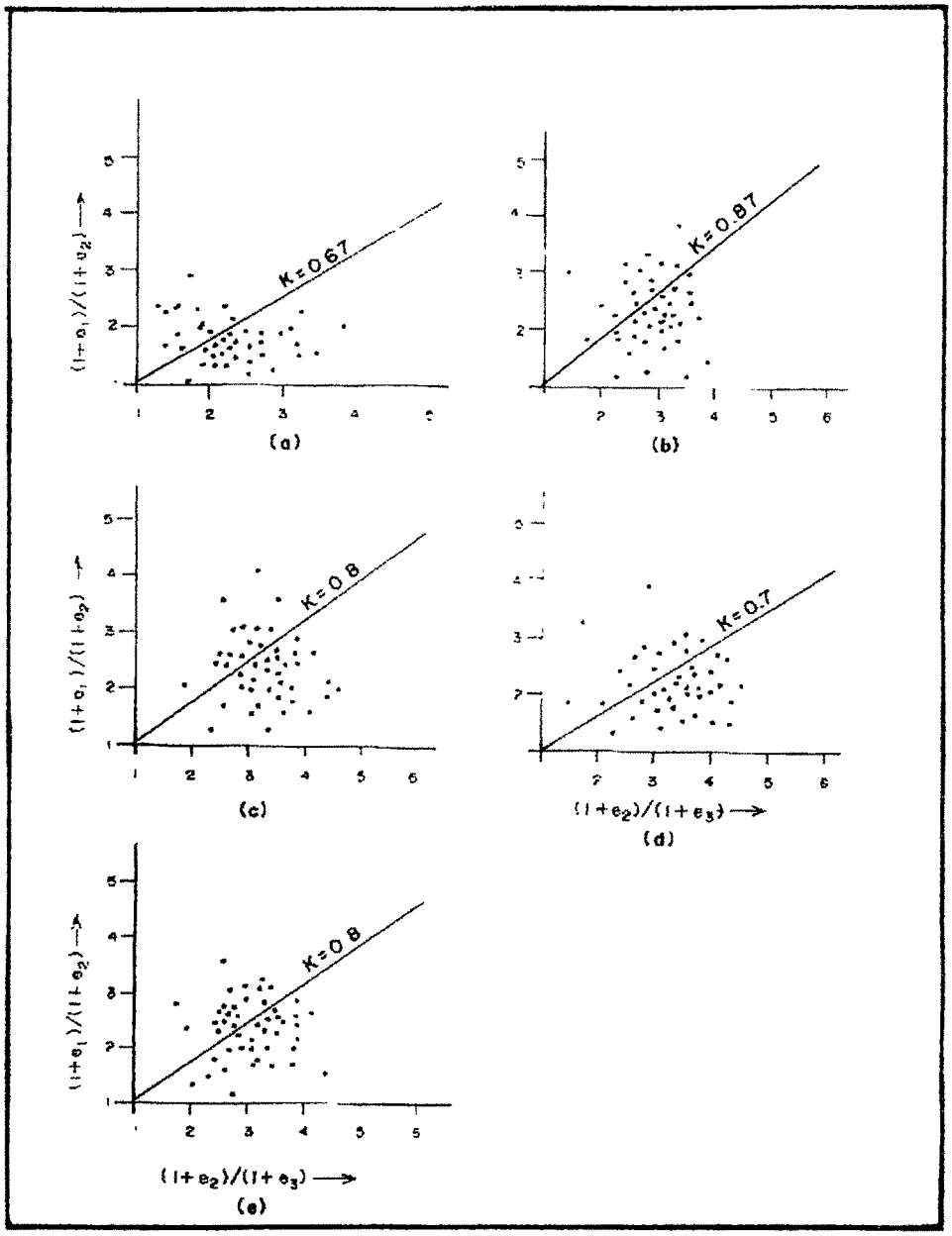

Fig. 4.27 — Plots of ratio of principal elongates (Flinn, 1962) for the Pebbles of Conglomerate.

a, b & c — Lulung Conglomerate

d, e — Mawryngkneng Conglomerate.

The natural logarithm of ratios of the principal strain $\log_e (1+e_1)/ (1+e_2) = \epsilon_1-\epsilon_2$, $\log_e (1+e_2)/ (1+e_3) = \epsilon_2-\epsilon_3$ and $\log_e (1+e_3)/ (1+e_1) = \epsilon_3-\epsilon_1$ are calculated, where $\epsilon = \log_e (1+e)$ and 'e' is the conventional strain given by $e = (\ell - \ell_0)/ \ell_0$, where ℓ = length after strain and ℓ_0 = length before strain (Nadai, 1950). The magnitude of strain can be expressed in terms of natural octahedral unit shear, γ_0 (Nadai, 1963). γ_0 represents the amount of shear along an octahedral plane where the axes of the regular octahedron are coincident with the principal strain directions. The amount of three-dimensional finite strain $\bar{\varepsilon}_s$ is thus determined by

$$\bar{\varepsilon}_s = \sqrt{3}/2.\ \gamma_0 \quad \text{(Nadai, 1963)} \text{ ----------(2)}$$

Where $\gamma_0 = 2/3[(\epsilon_1-\epsilon_2)^2+ (\epsilon_2-\epsilon_3)^2+ (\epsilon_3-\epsilon_1)^2]^{1/2}$

The symmetry of finite strain is described in terms of Lord's ratio 'v' [Hossack 1968] using the relation

$$V = (2\epsilon_2-\epsilon_1-\epsilon_3)/ (\epsilon_1-\epsilon_3) \text{ ---------- (3)}$$

In the present study, the principal extension $(1+e_1)$, $(1+e_2)$ and $(1+e_3)$ and the logarithmic strain ϵ_1, ϵ_2 and ϵ_3, were calculated. Using these basic parameters, the shape factor (κ), natural octahedral unit shear (γ_0), three dimensional finite strain ($\bar{\varepsilon}_s$) and symmetry of strain ellipsoid (v) were computed and the summarized data are given on (Table-4.5, 4.6, 4.7, 4.8& 4.9)

The measured axial ratios of deformed pebbles do not give the true bulk strain of the pebble of deformation because the final shape is also influenced by other factors which includes, (a) errors of measurement, (b) variation of composition, (c) original shape and orientation of the conglomerate pebbles prior to strain, (d) difference in ductility between the pebbles and their matrix, (e) change of volume during strain and (f) the effect of repeated deformation (Hossack 1968). Out of these factors, error produced by original shape factors

of the pebbles is probably the largest one encountered in measuring deformed conglomerate (Hossack 1968).

In the present study, the method suggested by Hossack, 1968 for correction of original shape factor has been applied. Hossack, 1968 considered the shape factor with the axial ratios of 2.17/ 1.52/ 1.00 (viz. X / Y / Z) as this is near the average of shapes of undeformed sandstone and quartzite pebbles. Because natural strain units can be simply added or subtracted to superpose two or more co-axial strains, this initial shape factor was converted to natural strains (ϵ_1= -0.40, ϵ_2 = +0.02 and ϵ_3 = +0.38) and then subtracted from the measured strains.

It is observed that all strain states may be represented on a 60^0 segment of a circle in which '$\bar{\varepsilon}_s$' is measured along a radius and 'v' is measured around the circumference as in Fig-4.28a,b,c and Fig-4.29a,b. The magnitude of the strain '$\bar{\varepsilon}_s$' and symmetry of the strain 'v' have been calculated and the data have been plotted on polar graph of Hsu, 1966 for the graphical representation of the finite strain (Fig-4.28a,b,c and Fig-4.29a,b). From these figures, it is clear that the majority of the plots lie in the flattening field close to the line of plane strain.

From the studied three dimensional strain analysis on the deformed conglomerates, it is observed that about 75% of the pebbles have 'κ' values between 1 and 0 and corresponding Lode's ratio 'v' between 0 and 1(Fig-4.28a, b, c and Fig-4.29a, b). The total spread of 'v' is between +0.75 to -0.50, '$\bar{\varepsilon}_s$' from +0.25 to +0.70. The 'v' value indicates that the pebbles has undergone mostly simple compression as displayed by cake-pebbles, though in some cases they show simple extension as displayed by rod pebbles. However, some of these extension and compression combinations may result

from calculation errors as already discussed. Lower value of '$\bar{\varepsilon}$' indicates that amount of pebble distortion is not very high.

The XY-plane of the pebbles is approximately parallel to the bedding (S_0). The flattening type of pebbles and presence of folds in the area indicate that the principal stress acted across the strike of rocks. This stress is probably responsible for the deformation of the pebbles of conglomerate. In some exposures the long axes of the pebbles are distinctly angular to S_0 plane indicating that the deformation was mild and it was not strong enough to bring XY plane of the pebbles parallel to S_0. This is also supported by the low value of '$\bar{\varepsilon}_s$' in the present study.

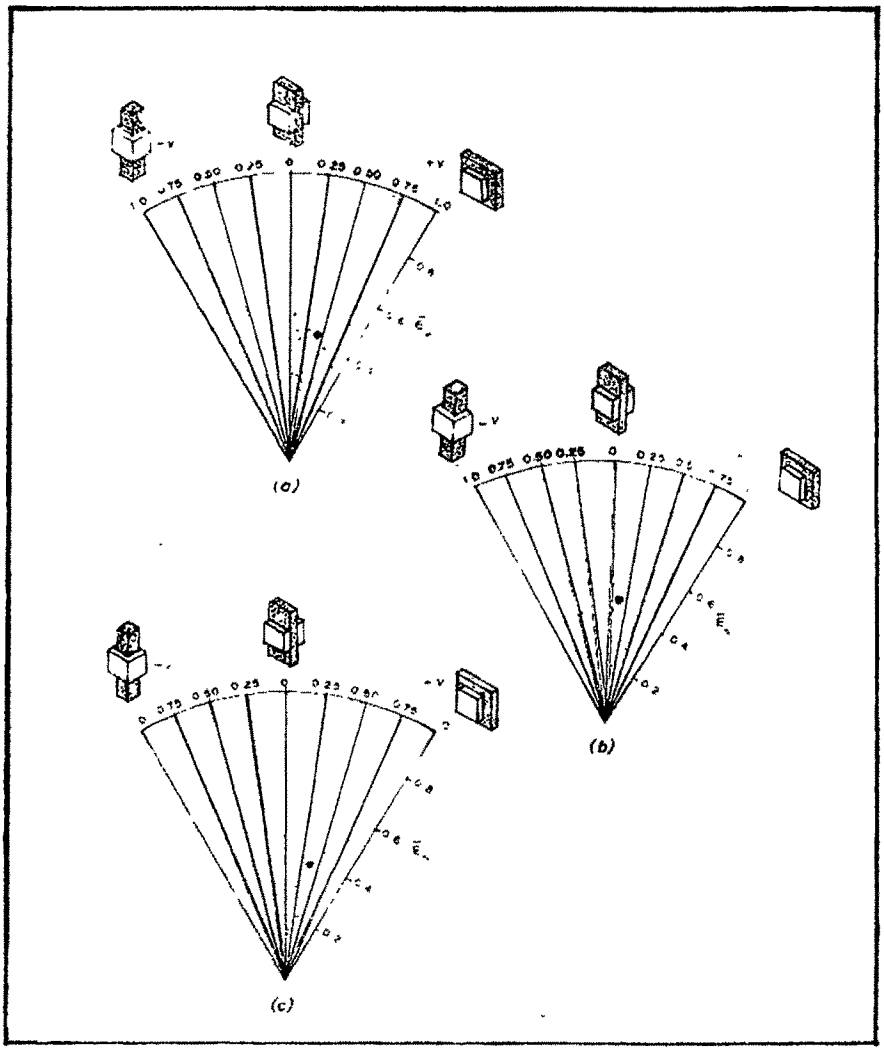

Fig 4.28 — Polar graph (HSu) of Lulung Conglomerate
(a),(b) & (c) — Polar graph exhibiting the variation in $\bar{\varepsilon}_s$ and V values (Table – 4.5), (Table – 4.6), (Table – 4.7)

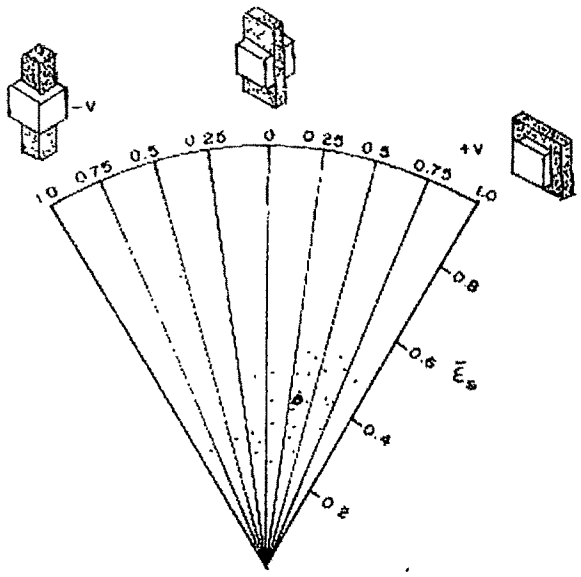

(a)

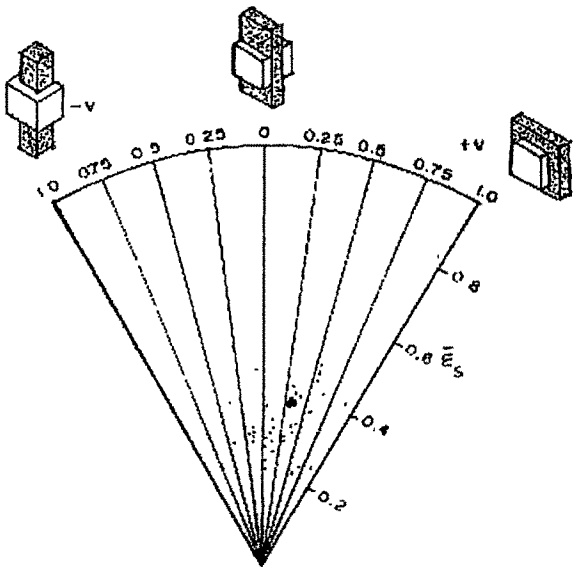

(b)

Fig. 4.29 — Polar graph (Hsu) of Maweyngkneng Conglomerate. (a),(b) Polar graph exibiting the variation in $\bar{\epsilon}_s$ and v values (Table — 4.8),(Table — 4.9)

4.6 Discussion and Tectonic History

The study of various structural elements and their mutual relationship has immensely helped in deciphering the tectonic history of the study area in particular and that of Shillong Group of rocks in general.

From the study of non-diastropic structure like current beddings, ripple marks, Graded bedding etc indicates the fluvial depositional regime of the time. The presence of structure produced by penecontemporaneous deformation reveals that the land mass was not stable at the time of deposition of sediments.

The Shillong Group is represented by low-grade metamorphic rocks deformed and metamorphosed initially from sedimentary and igneous rocks. The formation of major and minor folds with associated cleavages, and lineations are the resultant fabrics caused due to the impact of deformation and metamorphism. The structural analysis has revealed that the dominant foliation is trending in a NE-SW direction and dipping towards both NW and SE directions due to folding. The force responsible for such folding, might have probably acted from NW-SE direction. This is quite clear from the orientation of the dominant slaty-cleavage, flattening type of pebbles in conglomerate, joint orientation diagrams and trend of quartz veins.

The diastrophic structures observed in the rocks of Shillong Group reveal the four major phases of deformation (D) are noticed.

First phase of deformation (D_1): During the first phase of folding movement F_1 the sediments were subjected to different environment of deformation. The sub horizontal simple shear acted in NW-SE direction acting on horizontal

beds give rise to recumbent isoclinal F_1 folds with a NE-SW axial trend The development of early cleavage S_1 i.e. strong axial plane schistosity is associated with the formation of F_1 folds. The other associated structures formed are intersection lineation, mineral lineation etc.

Second phase of deformation (D_2): In the second phase of deformation minor open asymmetrical to symmetrical folds F_2 were developed due to refolding of S_0 and S_1 and where F_2 is generally co-axial with F_1 folds (Fig-4.18). This requires that the direction of shortening during the formation of F_2 folds is approximately perpendicular to the F_1 fold axes. Thus, the simple shear which gave rise to the F_1 folds gave place to pure shear with NW-SE compression which formed the F_2 folds with a northeasterly axial trend. The F_2 folds are associated with the development of slaty-cleavage or crenulation cleavage axial planar to the F_2 folds.

Third phase of deformation (D_3): The movements of third phase represent the last major event in the tectonic history of the area. This deformation is responsible for the development of large open symmetrical folds (synform) F_3, in the metasediments of the area. The maximum compression along NW-SE direction is responsible for the formation of F_3 fold. The another associated structures produced due to this phase of deformation are pukers, slikensides, kink bands, fracture cleavage S_3 etc.

Fourth phase of deformation (D_4): The fourth phase of deformation culminated in cataclasis which gave rise to deformation of rocks in the semi-brittle or brittle conditions. The deformation D_4 is related to the action of intrusive bodies of the area. This phase is responsible for the development of joints, fracture cleavage and crushing the rocks of the area.